STUDY OF MIXED, HETEROGENOUS FLOW OF POLYMER MELTS IN A CONVERGING CHANNEL DIE USING ELLIPTICAL CYLINDRICAL COORDINATES

By

RAJASEKHAR MALLIPEDDI

Bachelor of Technology

Regional Engineering College

Tiruchirapalli, India

April, 1992

Submitted to the Faculty of the
Graduate College of the
Oklahoma State University
in partial fulfillment of
the requirements for
the Degree of
MASTER OF SCIENCE
December, 1994

STUDY OF MIXED, HETEROGENOUS FLOW OF POLYMER MELTS IN A CONVERGING CHANNEL DIE USING ELLIPTICAL CYLINDRICAL COORDINATES

Thesis approved:

Thesis Advisor

Dean of the Graduate College

. . . . To my parents

ACKNOWLEDGEMENTS

I wish to express my sincere gratitude to my major professor, Dr. David Alan Tree. He gave me valuable career advice in addition to his service as my thesis advisor. I am deeply appreciative of his efforts on my behalf.

I wish to thank my parents for making it possible for me to come here and also for their constant motivation, caring and continuous support.

The financial support of the School of Chemical Engineering and the Polymer Research Group at Oklahoma State University is greatfully acknowledged.

PREFACE

A study of mixed, heterogenous flow in polymer melts has been conducted with a converging channel die. Elliptical cylindrical coordinates were used to effectively describe the stream lines in the converging channel. The components of the rate of strain tensor were calculated using the method of the stream function, and the functionality of the stream function was determined. The equation of motion and equation of continuity were derived for the elliptical cylindrical coordinate system. An attempt has been made to arrive at the rate of strain tensor without using strenuous experimental procedures like the tracer particle method. A procedure for calculating the stress fields was developed and the stress fields were calculated.

TABLE OF CONTENTS

LIST OF FIGURES

LIST OF TABLES

CHAPTER 1

INTRODUCTION

Polymeric materials are being widely used due to their superior performance over many other materials in broad ranging applications. In the production of polymeric components the most significant cost involved is the fabrication cost. One of the most important issues associated with polymer fabrication is the polymer melt flow behavior. In polymer processing operations, certain conditions give raise to unstable flow phenomenon, either limiting the production rate or giving rise to an unacceptable product. Hence the study of polymer melt rheology which is the primary focus of this thesis is essential for any processing related activities.

1.1 Significance

A description of the polymer melt rheology is essential to many polymer processing operations. Economical design of polymer processes depends on the accuracy of the rheological models used to relate the deformation rate of the polymer melt to the forces acting on the polymer melt. Many polymer processing operations

involve the use of extrusion dies (e.g., spinnerets and film dies) where the flow is converging. In converging channels, flows are mixed and heterogenous; meaning that extensional and shearing deformations occur simultaneously and that the deformation rate is spatially dependent. Currently available rheological equations of state generally account well for either extensional or shearing flow but not for mixed flow conditions. One strategy in designing a polymer process is to select the equation which suits the dominate deformation mode, which can lead to significant errors which are then dealt with empirically. Hence from a practical point of view a rheological equation of state for mixed, heterogenous flow is important.

From a theoretical point of view, knowledge of the rheological behavior of polymer melt gives a better understanding of the fundamental nature of the polymer molecules. Also, converging flow, representing a non viscometric flow, and will provide an opportunity for testing the usefulness of various constitutive equations under conditions other than viscometric flow. Viscometric flow is rheologically steady shear flow.

1.2 Objectives

The overall objective of the project, of which this thesis is a part, is to develop a single, if possible, simple rheological equation of state which suitably describes polymer melts in mixed, heterogeneous flow conditions. This thesis supports the overall goal by using a new coordinate system to describe the flow of polymer melts

more accurately in a converging channel and by demonstrating how the stress fields and flow kinematics can be determined independently. One of the main objective of the thesis is to prove that working in the elliptical cylindrical coordinate system is more convenient than the cylindrical coordinate system used in previous studies (Han & Drexler, 1973c; Yoo & Han, 1981) to describe the flow kinematics. The other objectives are to calculate the stress fields from flow birefringence data and to formulate a method to calculate flow kinematics without using strenuous experimental procedures.

1.3 Thesis Organization

This thesis is divided into five chapters. Chapter 1 gives a brief introduction. Theoretical developments and relevant background information are discussed in Chapter 2. The experimental set up and techniques are discussed in Chapter 3. The results and discussions are in Chapter 4. Chapter 5 states the conclusions and gives recommendations for future work.

CHAPTER 2

BACKGROUND

This study requires a background in several topics such as flow through converging channels, flow birefringence, the stress optic relation and flow kinematics. The relevant ideas on each subject area are reviewed in this chapter.

2.1 Converging Flow

Converging flow is one of the most important flow geometries encountered in industrial processes involving polymer melts. In a converging channel, shear stresses and elongational stresses coexist with the additional characteristic that the flow is heterogenous. Flow of polymer melts in converging channels has been studied by many researchers (Cogswell, 1972; Han & Drexler, 1973a; Han & Drexler, 1973b; Han & Drexler, 1973c; Yoo & Han, 1981) in an effort to enhance the understanding of the stress distributions of polymer melts in a converging channel. Han, Drexler and Yoo (Han & Drexler, 1973a; Han & Drexler, 1973b; Han & Drexler, 1973c; Yoo & Han, 1981) have studied flow through converging channel for a tapered die

entrance and for a sudden contraction. The method of birefringence was used to determine the stress fields, and the streak photography method was used to determine the kinematics. The cylindrical coordinate system was used by Han, Drexler and Yoo to describe the stream lines. Using a modified second order fluid model, equations of motion were solved in cylindrical coordinates, to arrive at the velocity fields as a function of the volumetric flow rate and converging angle of the channel. The equation Yoo derived for the converging channel was

$$v_r(r,\theta) = \left(\frac{\cos 2\theta - \cos 2\alpha}{1 - \cos 2\alpha}\right)\frac{f(0)}{r} \qquad (2.1)$$

where α = converging angle of the die,

r, θ = Cylindrical coordinates.

In Eq. 2.1, f(0) is related to the volumetric flow rate per unit length of channel width, Q, and was determined from the following equation

$$Q = -2\int_0^{\alpha} v_r(r,\theta) r d\theta = \left(\frac{2\alpha\cos 2\alpha - \sin 2\alpha}{1 - \cos 2\alpha}\right) f(0). \qquad (2.2)$$

Eq. 2.1 was used to calculate the stress fields which were compared to the experimentally calculated stress fields. The results of the comparison indicated that the modified second order model predicted stresses that were approximately the same order of magnitude as the experimentally determined stresses. However, the patterns of the predicted stresses were not similar to the experimental profiles.

2.2 Flow Kinematics

Flow behavior can be distinguished by looking at the elements of the rate of strain tensor. In two dimensional flow the rate of strain tensor can be represented as follows:

$$\dot{\gamma} = \begin{pmatrix} a & b & 0 \\ b & -a & 0 \\ 0 & 0 & 0 \end{pmatrix}, \tag{2.3}$$

where a and b may be functions of position.

In Eq. 2.3, if 'b' is the only non-zero then the flow is termed simple shear. If 'a' is only non-zero component then the flow is termed planar extensional. If 'a' and 'b' are spatially dependent then the flow is heterogeneous. In this study of flow of polymer melts through converging channels 'a' and 'b' were generally non-zero and spatially dependent. Hence the flow was mixed heterogeneous.

2.3 Flow Birefringence

The method of isoclinics to determine stress fields in polymer melts is based on the fact that some materials are optically anisotropic, meaning that the material has directionally dependent optical properties. The refractive index in an orthorhombic crystal cell is an example of an optically anisotropic material. In an orthorhombic

material the density is different in different directions which causes a difference in refractive index. In polymer melts, birefringence arises from the stress difference.

Birefringence is defined as the difference in refractive index along the first and second principle optical axes of a material. Birefringence can be visualized as polarized light entering an optically anisotropic medium and splitting into two beams (the ordinary and extraordinary beam), which travel along the axes at different speeds. When the two beams emerge from the medium they have a certain relative phase difference, R, which is given by (Tree, 1991):

$$R = \frac{L}{\lambda}[n_{p1} - n_{p2}] = \frac{L\Delta}{\lambda} \tag{2.4}$$

where

L = thickness of the medium,

λ = wave length of light used,

n_{p1} = first principal refractive index,

n_{p2} = second principal refractive index,

Δ = birefringence.

Closely related to the phase difference, R, is the retardance, δ, which is given by (Tree, 1991)

$$\delta = 2\pi R. \tag{2.5}$$

Polymer melts are known to be birefringent when subjected to stress. This

property of the polymeric melts has led to the empirical observation called the stress optic relation developed by Newmann and Maxwell (Janeschitz-Kriegl, 1983). The stress optic relationship assumes that:

(i) the principal axes of the stress tensor is collinear with the principal axes of the refractive index tensor or mathematically

$$\chi_m = \chi_0 = \chi, \tag{2.6}$$

where

χ_m = orientation angle of stress,

χ_0 = orientation angle of the refractive index tensor, and

χ = isoclinic angle and

(ii) the birefringence at any point is linearly proportional to the first principle stress difference in the plane perpendicular to the axis of light propagation.

Therefore:

$$\Delta = C(\tau_{p1}-\tau_{p2}), \tag{2.7}$$

where

C = stress optic coefficient,

τ_{p1} = first principle stress,

τ_{p2} = second principle stress.

Eq. 2.7 suggests that Δ is a function only of the difference of two principal

stresses in the plane perpendicular to the axis of light propagation. The validity of the linear assumption has been shown by several studies, particularly at low deformation rates (Han & Drexler, 1973b; McHugh, Mackay, & Khomami, 1987; Janeschitz-Kriegl, 1983).

From Eqs. 2.6 and 2.7, the shear stress and first normal stress difference can be calculated from photoelastic measurements. The stress components can be transformed from the principal coordinates to the laboratory coordinates by rotating the principle stress tensor in the counter clockwise direction (which is considered positive) through an angle χ. The transformation yields shear stress and first normal stress difference as follows:

$$\tau_{12} = \frac{\tau_{p1}-\tau_{p2}}{2}\sin(2\chi), \tag{2.8}$$

$$\tau_{11}-\tau_{22} = (\tau_{p1}-\tau_{p2})\cos(2\chi). \tag{2.9}$$

Substituting Eq 2.7 into Eqs. 2.8 & 2.9 gives

$$\tau_{12} = \frac{\Delta}{2C}\sin(2\chi), \tag{2.10}$$

$$\tau_{11}-\tau_{22} = \frac{\Delta}{C}\cos(2\chi) \tag{2.11}$$

where

τ_{12} = shear stress,

$\tau_{11} - \tau_{22}$ = first normal stress difference.

If Δ ,C ,χ are known then the shear stress and first normal stress difference can be calculated.

The fraction of transmitted light, Tr, as a function of birefringence and isoclinic angle for the optical train used in this study was derived by Tree (Tree, 1990):

$$Tr = \frac{1}{4}\sin^2\left(\frac{\pi L\Delta}{\lambda}\right)[1 - cos4(\chi - \alpha)], \qquad (2.12)$$

where α is the polarizer angle.

The sin term is known as the isochromatic term and the cos term is known as the isoclinic term. When the value of the argument of the isochromatic term is an whole number multiple of π, the value of the isochromatic term is zero and the resulting total extinction of light is called an isochromatic band. The isoclinic bands occur when there is total extinsion due to isoclinic term i.e., when $\alpha = \chi$. The stress optic coefficient can be found from the position of the isoclinics and isochromatics in a well characterized flow of a polymer melt such as a slit flow die. In Eq. 2.10, the shear stresses in a well developed flow are calculated from the pressure gradient and Δn, χ are calculated from the position of isoclinics and isochromatics. A plot of shear stress as a function of $\Delta n \sin(2\chi)$ gives a straight line, the slope of which is

1/2C.

2.4 Elliptical Cylindrical Coordinates

The elliptical cylindrical coordinate system is shown in Figure 2.1. A point is represented in this coordinate system by the intersection of a hyperbola of constant η and a cylinder of constant Ψ. Elliptical cylindrical coordinates are related to rectangular coordinates by

$$x = a \cosh\psi \cos\eta, \tag{2.13a}$$

$$y = a \sinh\psi \sin\eta, \tag{2.13b}$$

$$z = z. \tag{2.13c}$$

Eqs. 2.13a and 2.13b can be rearranged to give

$$\frac{x^2}{\cos^2\eta} - \frac{y^2}{\sin^2\eta} = a^2. \tag{2.14}$$

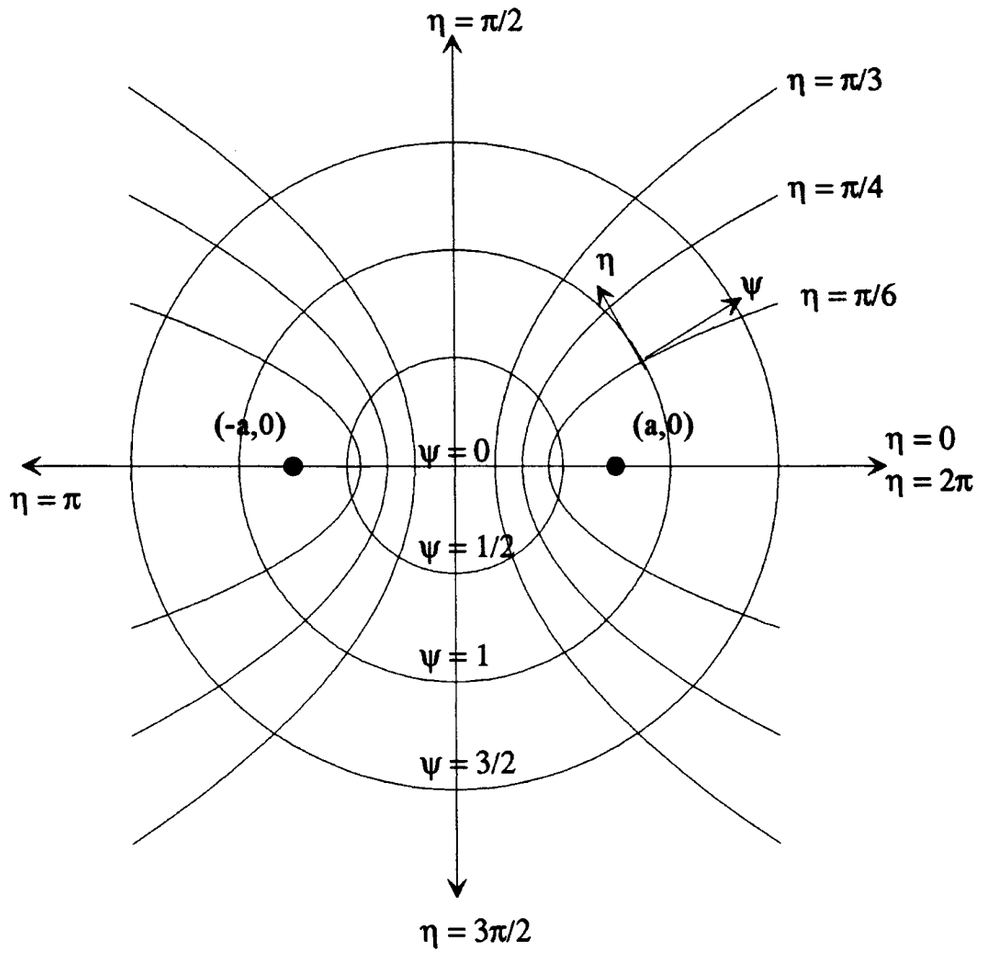

Fig 2.1: Elliptical Cylindrical Coordinates

Eq. 2.14 can also be written as

$$y^2 = \tan^2\eta \; x^2 - c\sin^2\eta, \tag{2.15}$$

where $c = a^2$.

Eq. 2.15 facilitates the conversion from the rectangular coordinates. In this study elliptical cylindrical coordinates were used to describe the stream lines, instead of the cylindrical coordinates which were in common use for a converging channel.

CHAPTER 3

EXPERIMENTAL

The primary goal of the experimental work in this thesis was to obtain independently the kinematics and stress fields in heterogenous, mixed flows of polymer melts. For the completion of the work the following measurements were necessary:

(i) the stress optic coefficient of the polymer melts has to be calculated and

(ii) the flow birefringence, and the polymer flow has to be recorded clearly.

In order to obtain the stress optic coefficient, the birefringence, isoclinic angle and the shear stress must be simultaneously measured, which can be achieved by providing a region where there is a fully developed shear flow. The flow birefringence and polymer flow can be seen clearly by providing glass windows.

This chapter describes the experimental equipment, polymeric materials, techniques and procedures used for this experimental work.

3.1 Equipment

3.1.1 Die

The following die features were required to produce mixed and pure shear flow conditions; allow the observation of flow birefringence; and measure the pressure gradient;

(i) a converging channel with variable angle of convergence to assure a mixed, heterogenous flow,

(ii) a rectangular slit section which begins at the point where the converging channel ends, to produce a well characterized shear flow.

(iii) glass windows in the slit flow and the converging section to allow for observation of the birefringence and streamlines.

(iv) pressure traducers, to measure the pressure gradient, mounted in the slit flow section.

(v) thermocouples to measure the melt and die temperatures.

The slit flow die used was the same as described by Ajai (Ajai, 1992). The die was built according to the specifications of this project in the Physical Sciences machine shop and is depicted in Figure 3.1. The die was made of stainless steel except for the wedges in the converging channel which were made of brass, and the glass windows.

The die was an assembly of nine parts, seven of which are shown in Figure

3.1. One of the rectangular strips (38.2 cm x 5 cm x 3.75 cm) contained the 0.254 cm x 2.54 cm channel and was used as the lower plate. To minimize the wall effects, the aspect ratio, the ratio of depth to width, was chosen as 10:1. The selection of this aspect ratio was based on the work by McHugh, Mackay and Khomami (McHugh, Mackay, & Khomami, 1987) who showed that the wall effects are minimized when the ratio is equal to or greater than 10:1. Another plate of the same dimension was used as the upper plate.

The window in the converging section had a diameter 5.04 cm and the small window in the slit flow section had a diameter 2.54 cm. These two plates, containing the window wells and the assembly shown in Figure 3.1, were flanked by two other plates not shown in Figure 3.1 which kept the glass windows in position. A thermocouple well was drilled to allow measurement of the die temperature. Holes for mounting the pressure transducers are drilled in the upper plate. In order to check if the pressure transducers were mounted flush, one of the transducer holes was located so that the transducer can be seen through the windows.

Strain free optical windows made of laboratory grade glass were mounted in the window wells. The windows were coated with a anti-reflective coating to improve image quality. Care was taken to ensure that the windows are seated flush in the window wells, using adjustable screw type metal brackets, to prevent a three dimensional flow. Also thin metal wires were placed between the bracket and the glass windows to function as cross wires. To cushion the windows against possible stresses, thin Teflon gaskets were placed between each window and the plates that

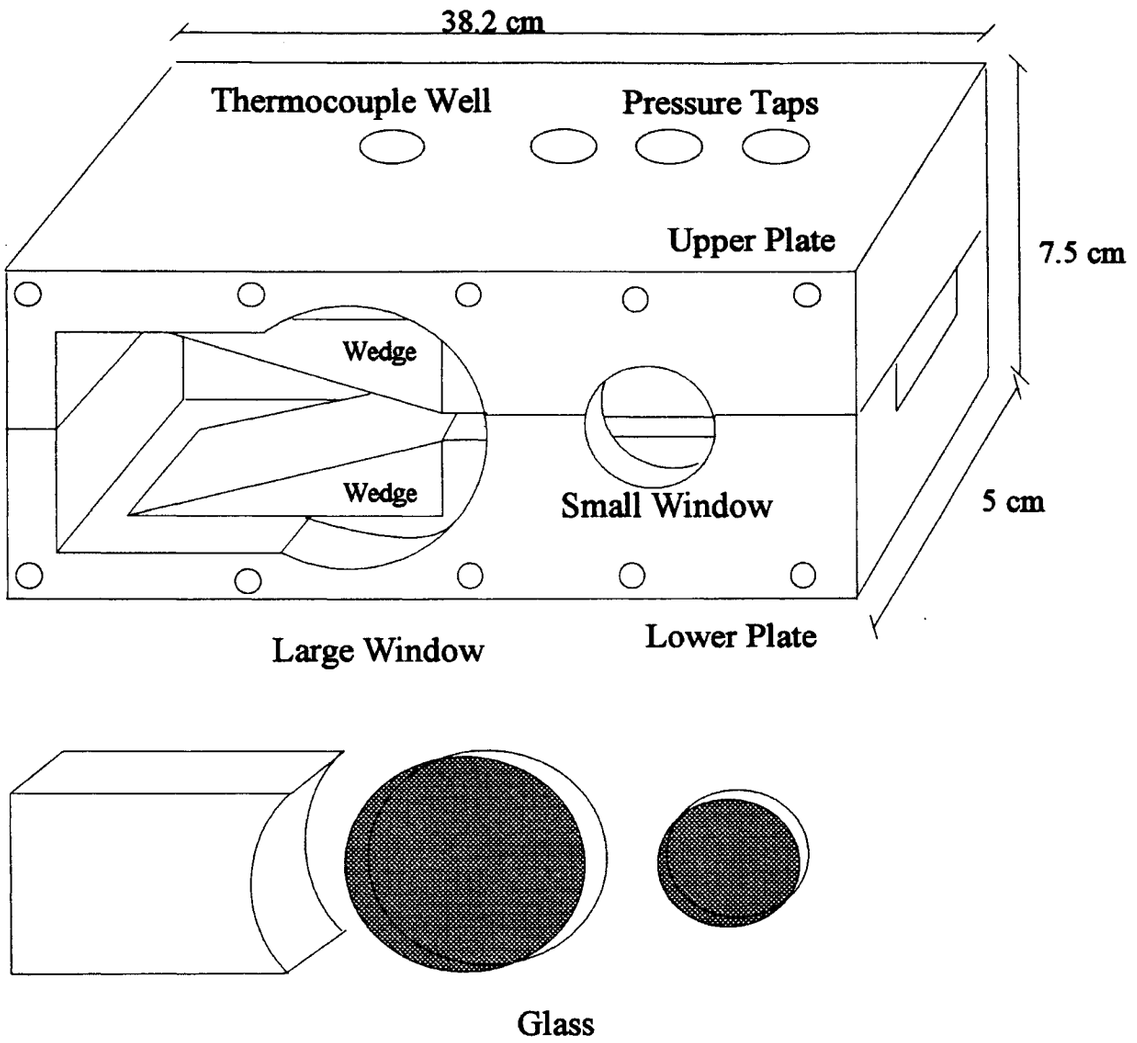

Figure 3.1: Pictorial View of the Die

flank the assembly. Heavy duty aluminum foil along with a high temperature sealant, were used to prevent leaks between the die parts.

The die was heated using a insulated fibre glass tape. The temperature was controlled to the desired value by connecting the tape to a temperature controller on the extruder. A combined temperature and pressure transducer (TPT 432A Dynisco) was mounted in the middle one of the three pressure taps. Two other pressure transducers (PT 422A Dynisco) were mounted in the other pressure taps.

3.1.2 Extruder

The extruder was a Killon polymer extruder with a 1 inch screw (model number KLB-100). The screw section was heated by three different heaters which were marked as zones 1 to 3. Each zone had a separate temperature controller. An outlet was provided on the extruder to plug in the heater coil for the die. An additional feed back temperature controller was present to control the temperature of the die. A thermocouple was provided to read the polymer melt temperature in the screw.

3.1.3 Optical and Video Set Up

The optical setup used was the same as that described by Ajai (Ajai, 1992) and is shown in Figure 3.2. The setup consists of a light source, collimating lens, filter,

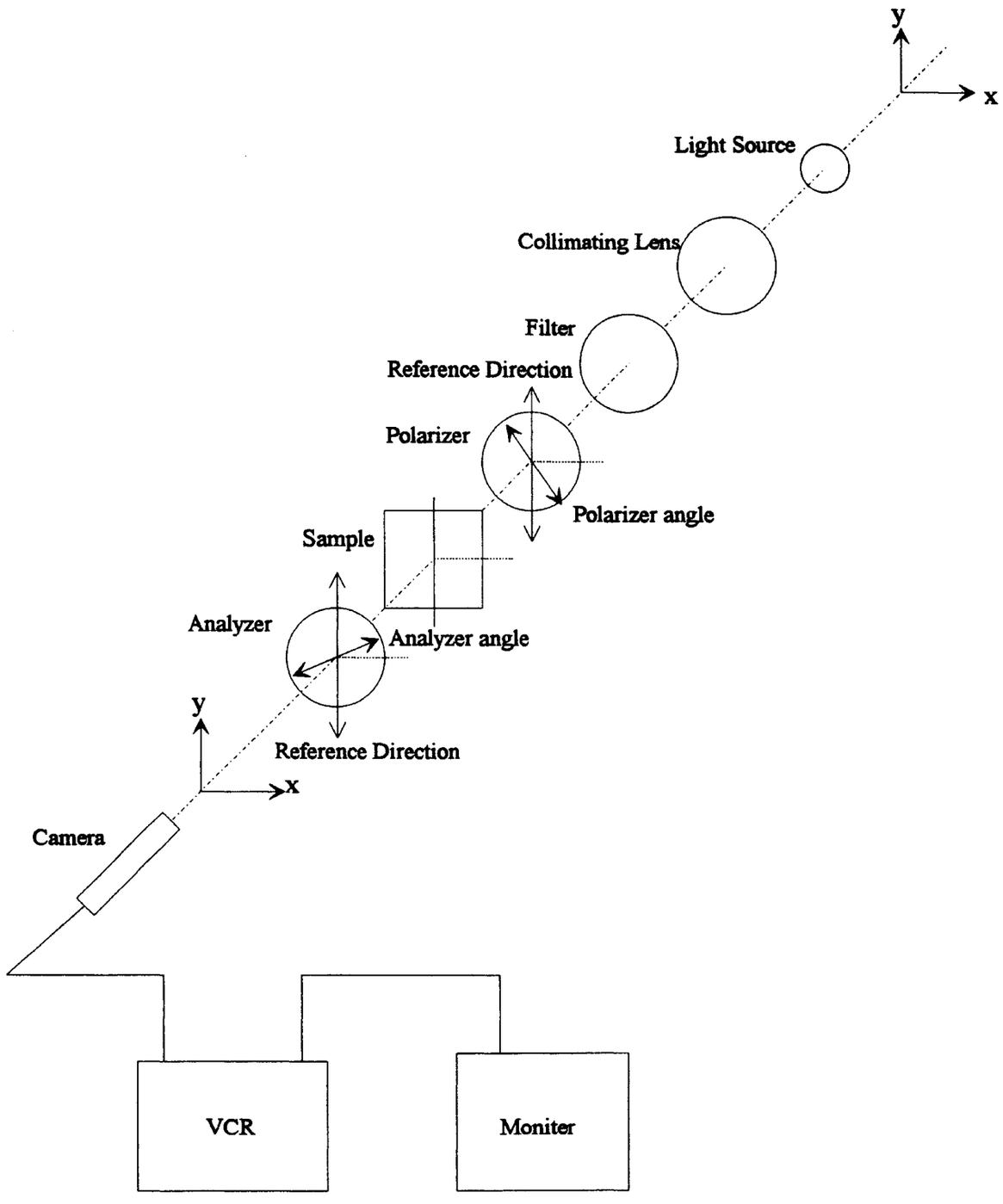

Figure 3.2: Optic and Video Setup

polarizer, sample, and analyzer all mounted on a aluminum optical rail.

The light source was a 150 W incadesent light bulb with a fiber optic light pipe 0.635 cm. in diameter which allowed the light to be delivered to the beginning of the optical train. The collimating lens was used to produce a parallel beam of light and was 75 mm. in diameter with a clear aperture of 70 mm, and had a focal length of 150 mm. The light source was placed at the focal point of the lens. The light filter had a maximum transmission at 488 nm, i.e. blue light, with a band width at half the height of peak, of 7.2 nm and a maximum transmission of 45%. The polarizer and analyzer were 101.6 mm in diameter with a clear aperture of 96 mm. Each polarizer was equipped with a circular scale to determine the polarizer orientation angle. The analyzer was "flipped" such that the orientation angle on the scale reads 0° when it is actually at an angle of 90°, to the polarizer, which facilitated the observation of the isoclinic bands while obtaining isoclinics.

The video set up consisted of a black and white video camera, a monitor and a VCR. The video camera was a black and white Javeline NEW VI CHIP CCD. The monitor was a black and white Javeline (model number BWM12). The VCR was a RCA VCR (model number VR520) equipped with additional features like frame by frame advance and speed control playback which simplified the analysis.

3.2 Materials

The polymer resins used are listed in Table 3.1 along with some selected

Polymer Materials

Material	Melt Index[2]	Density[2], (g/cm[3])	Melting Point[2], °C
GB 501-010 LLDPE (Quantum Chemicals)	1.0	0.919	120
LB 8510-00 HDPE (Quantum Chemicals)	1.3	0.960	131
Styron 656-D PS (Dow)	8.0	–	210[1]

1. Vicat softening point
2. Manufacturers data

Table 3.1 : Materials Used

physical data. This data were taken from the material safety data sheets provided by the manufacturer.

3.3 Techniques and Procedures

The extruder was started by switching on the power to the extruder. The temperatures for the different zones of the screw and the die were set according to the operating temperature of the die. For example, the temperatures for HDPE resin operating at 150 °C would be, 130, 140, 150, 150 °C, in zones 1, 2, 3 and the die respectively. Once the set temperatures are attained, the pressure transducers were calibrated. Before the screw was started, the rotation rate of the screw was set to zero and the feeder bin was checked to see if there was sufficient polymer feed. The screw was then started and the rotation rate increased to obtain the desired flow rate (The rotation rate reading was approximately equal to the volumetric flow rate in cc/min). The optical train was set up as shown in the Figure 3.2. All of the optical components were adjusted to the same height. The camera was adjusted to be perpendicular to the flow and was then focussed on the center of the channel using the cross wires. In order to focus the camera on the center of the channel, the camera was first focussed on the front cross wire then on the crosswire at the back and an average of the two positions was used.

3.3.1 Stress Field Data

The stress field data was obtained from the birefringence patterns. The birefringence pattern was recorded from the start of the flow with the polarizer and the analyzer at an angle of zero to the reference direction. This procedure was essential since the order of the isochromatic bands was determined from observing the birefringence pattern at the start of the flow. After the flow became steady the polarizer/analyzer angle was increased in 5° increments, by rotating the polarizer and the analyzer counter clockwise in unison. The birefringence patterns were recorded for approximately 30 seconds at each polarizer/analyzer angle up to 90°. The isochromatics and the isoclinics are then mapped using an image processing software called IRIS-T.

3.3.2 Using IRIS-T

IRIS-T is an image processing software package used to digitize images. An image is composed of an array of picture elements called pixels, arranged in 480 rows and 512 columns. Each pixel is characterized by its gray value. A gray value is a measure of the brightness and given by an integer that varies from 0 to 255 inclusive. A gray value of 0 corresponds to complete darkness while a value of 255 corresponds to complete light. Using IRIS-T a single frame in a video recording can be grabbed and displayed on screen. Then a cursor can be placed on the image and the gray

value at any pixel can be determined. There are two buffers located on the C drive, that can be used to store the images for easy retrieval. The following are some of the commands available in the IRIS-T software:

(i) Display Camera: This command displays the output from a VCR or Camera

(ii) Display Buffer {#}: Displays an image stored in a Buffer #.

(iii) Place_Cursor: Grabs a frame, displays it on the monitor and places a cursor on the monitor screen. Also pixel number (the row and column number in the array of pixels) and the gray value of that pixel are displayed on the computer screen.

The isolinics and isochromatics were mapped using the following procedure:

(i)The tape with the birefringence recording was played on the VCR;

(ii)An image was grabbed, displayed on the screen and a cursor was placed on the screen using the command Place_cursor;

(iii)The cursor was moved horizontally to the column number 30;

(iv)The cursor was moved along this column to the edge of a band (dark or bright);

(v)The darkest or the bright position of a band was then determined by moving the cursor up and down and finding the row number with the lowest or the highest gray value;

(vi)This row number was then noted as the position of the band in that column;

(vii) The procedure from (iv) to (vi) was then repeated for all the bands;

(viii)The cursor was then moved to near the edge of the die;

(ix)The edge of the die was marked as the position where there is a sudden change in gray value;

(x) The above two steps were repeated for the other edge of the die;

(xi) Steps (iii) to (x) were then repeated for column numbers 60 to 360 in increments of 30.

(xii) The pixel values were then converted to the actual positions, by using the number of pixels between the edges at the mouth of the die as a basis.

(xiii) Upon completion of this procedure, the positions were plotted to give isochromatics and isoclinic contours.

3.3.3 Kinematics Data

The flow kinematics were obtained from tracer particle data. To get the tracer particle data, the flow was recorded without the polarizer and the analyzer for approximately 20 minutes. The VCR was set to record at the fastest possible speed to give a good picture quality. The tapes were analyzed frame by frame. The inherent impurities in the polymer resin were used as tracer particles.

The video tapes were analyzed in the following way:

(i) A transparency was taped on to the monitor screen;

(ii) The VCR and monitor are turned on;

(iii) The flow was carefully examined and the particles which stayed clearly focussed while passing through the channel were selected;

(iv) The time required for each particle to go from one end of the screen to the other was noted;

(v) Depending on the time determined in step iv, the position of the particle was marked on the transparency at time intervals such that fifteen to twenty tracer particle positions could be obtained for each streamline(for example every 1/3 sec or 10 frames etc.,);

(vi) This procedure was repeated for different tracer particles;

(vii) The horizontal and the vertical distances of the particles from the center of the slit die entrance were measured manually.

The data obtained for each tracer particle was fitted to the Eq. 2.15 using the following procedure:

(i) The data was entered into an Excel spread sheet.

(ii) y^2 was plotted as a function of x^2 and fit to a straight line. The value of c and η where determined from:

$$Slope = \tan^2\eta \tag{3.1}$$

$$Intercept = -c \sin^2\eta \tag{3.2}$$

where c and η are constant.

Using calculated values of c and η, the predicted y values and the corresponding x values were then plotted to give ideal elliptical cylindrical fits. When the reference point (or the origin) was taken as the entrance of the die, the

predicted y values for points inside the mouth of the die were roots of a negative numbers. Therefore, the reference point was moved .5 cm, in the negative y-direction, into the mouth of the channel and the data was fit to Eq. 2.15 as described above. The predicted y values were then calculated and if some of the values were still imaginary, the reference point was moved further into the mouth of the channel. This procedure was repeated until all the predicted y values were real. Since the field of view of the camera was approximately same for all of the experiments, the number of tracer particles observed in the mouth if the converging channel was the same. Therefore once a reference point was determined for a given experiment, the same point could be used for all other experiments.

Chapter 4

RESULTS AND DISCUSSION

The results of the rheo-optic analysis of the mixed heterogenous polymer flow are presented in this chapter. The elliptical cylindrical coordinate system was used to give a better representation of the stream lines in a converging channel. The equations required to work in elliptical cylindrical coordinate system were derived and presented. Flow kinematics were calculated using the method of stream functions in elliptical cylindrical coordinates. An extensive study on the observed birefringence patterns was conducted and the stress fields were obtained.

4.1 Stream Line Data

In this section the results of the study of converging channel kinematics are presented. Elliptical-cylindrical coordinates were used to describe the stream lines in the converging section.

The plot in the Figure 4.1 depicts the path of different tracer particles for LLDPE at 165 °C, 16 cc/min and an 30° angle of convergence. The solid lines

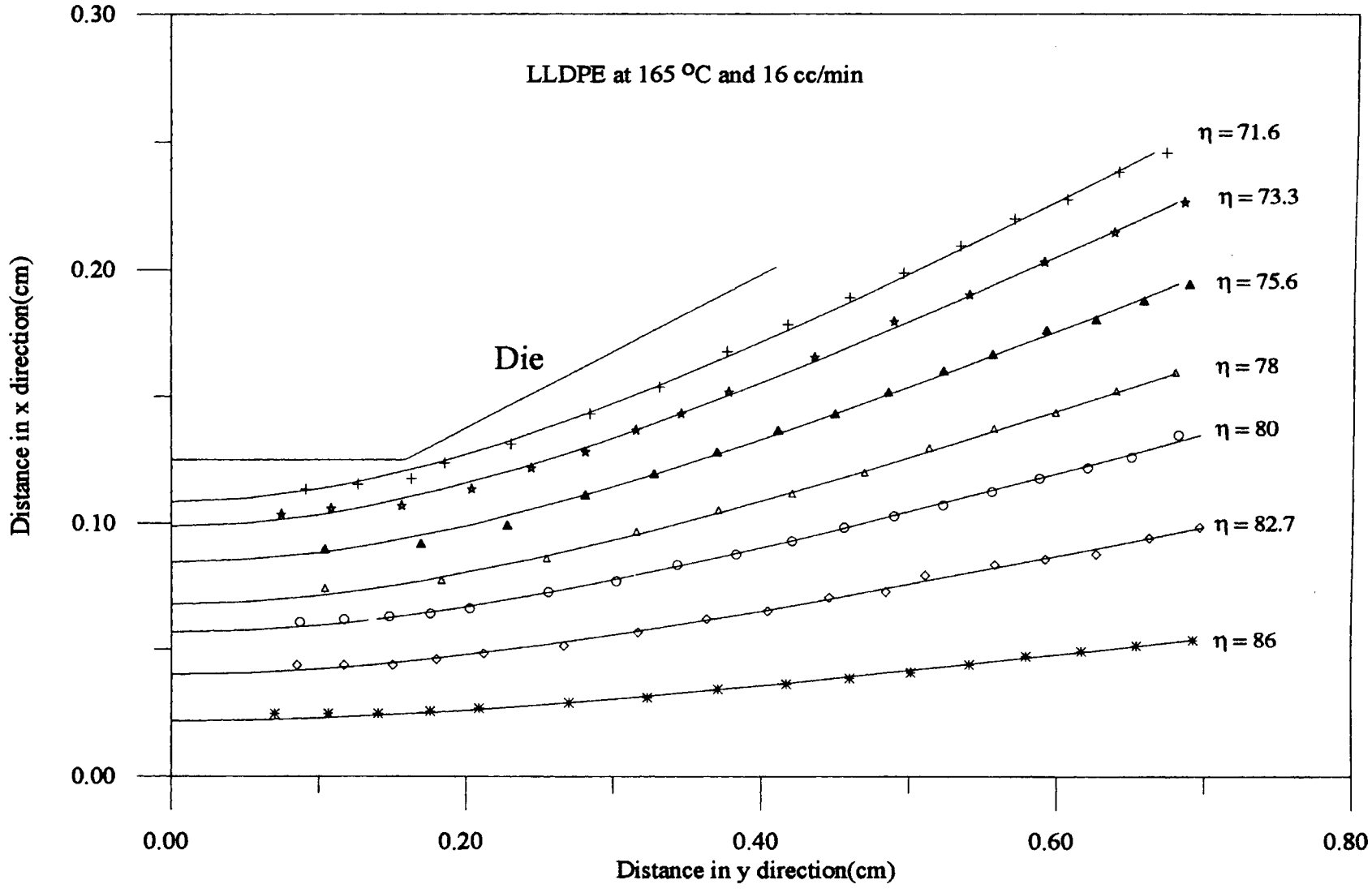

Fig 4.1 : Streamlines Fit to Elliptic Cylindrical Coordinates

shown in Figure 4.1 are best fits of the tracer particles data to Eq. 2.14. These solid lines are lines of constant η. The horizontal and vertical distances were measured from a reference point 0.16 inches into the slit flow region, along the center of the channel. The data points indicate the position of the tracer particles at any given time.

Figures 4.2 to 4.4 show representation plots of the stream lines in elliptical cylindrical coordinates, for different temperatures, flow rates and materials. Additional plots of stream lines appear in Appendix E. Figure 4.2 shows the stream lines for LLDPE at 150 °C and 10.7 cc/min. Figures 4.3 shows the stream lines for HDPE at 165 °C and flow rate of 6 cc/min. Figure 4.4 shows the stream lines for HDPE at 165 °C and a flow rate of 20 cc/min in both elliptical cylindrical and cylindrical coordinates. The ideal elliptical cylindrical paths are denoted by thick solid lines and the ideal cylindrical paths by thin solid lines. The stream lines described by elliptical cylindrical coordinates are better representations of the path traced by the particles than the cylindrical coordinates, as seen from the Figure 4.4 particularly at the entrance region of the converging channel.

The following observations can be made from the Figures 4.1 to 4.4:

(i)As required by the law of continuity, the streamlines do not intersect;

(ii)The stream lines are lines of constant η and c;

(iii) The tracer particles near the wall show the greatest deviation from ideal paths at the entrance to the slit flow section.

(iv) The stream lines described by elliptical cylindrical coordinates are a better

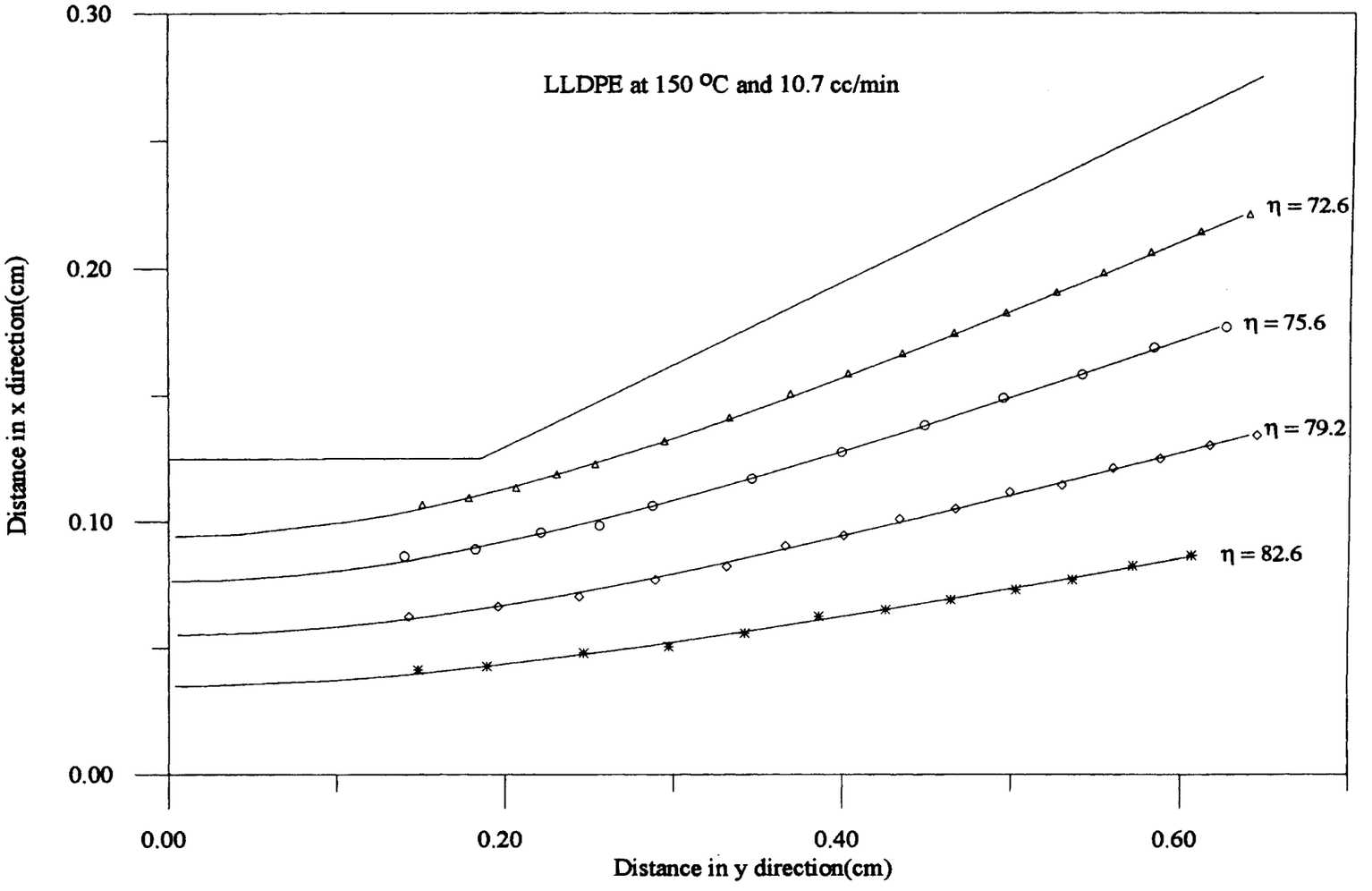

Fig 4.2 : Streamlines Fit to Elliptic Cylindrical Coordinates

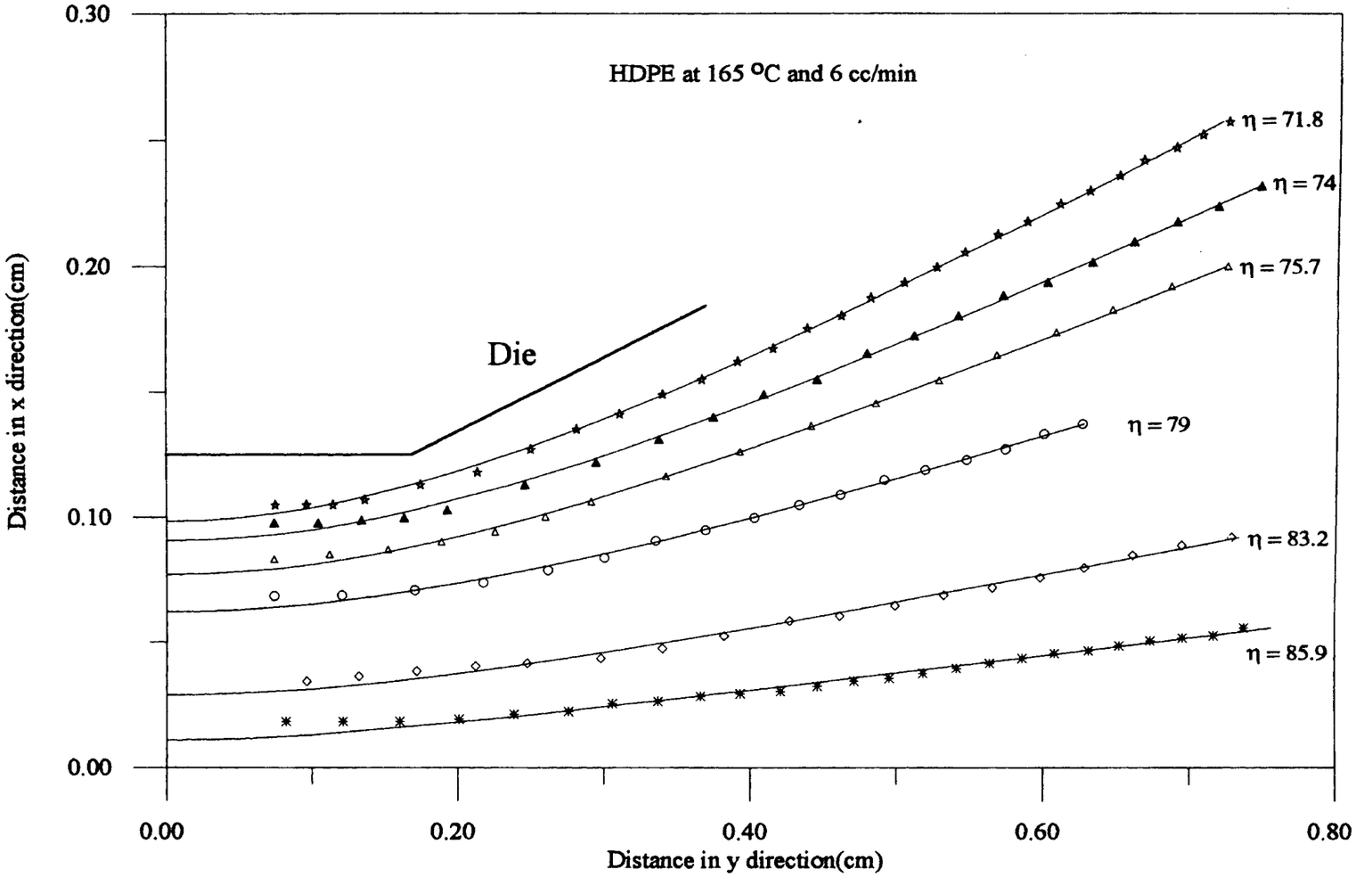

Fig 4.3 : Streamlines Fit to Elliptic Cylindrical Coordinates

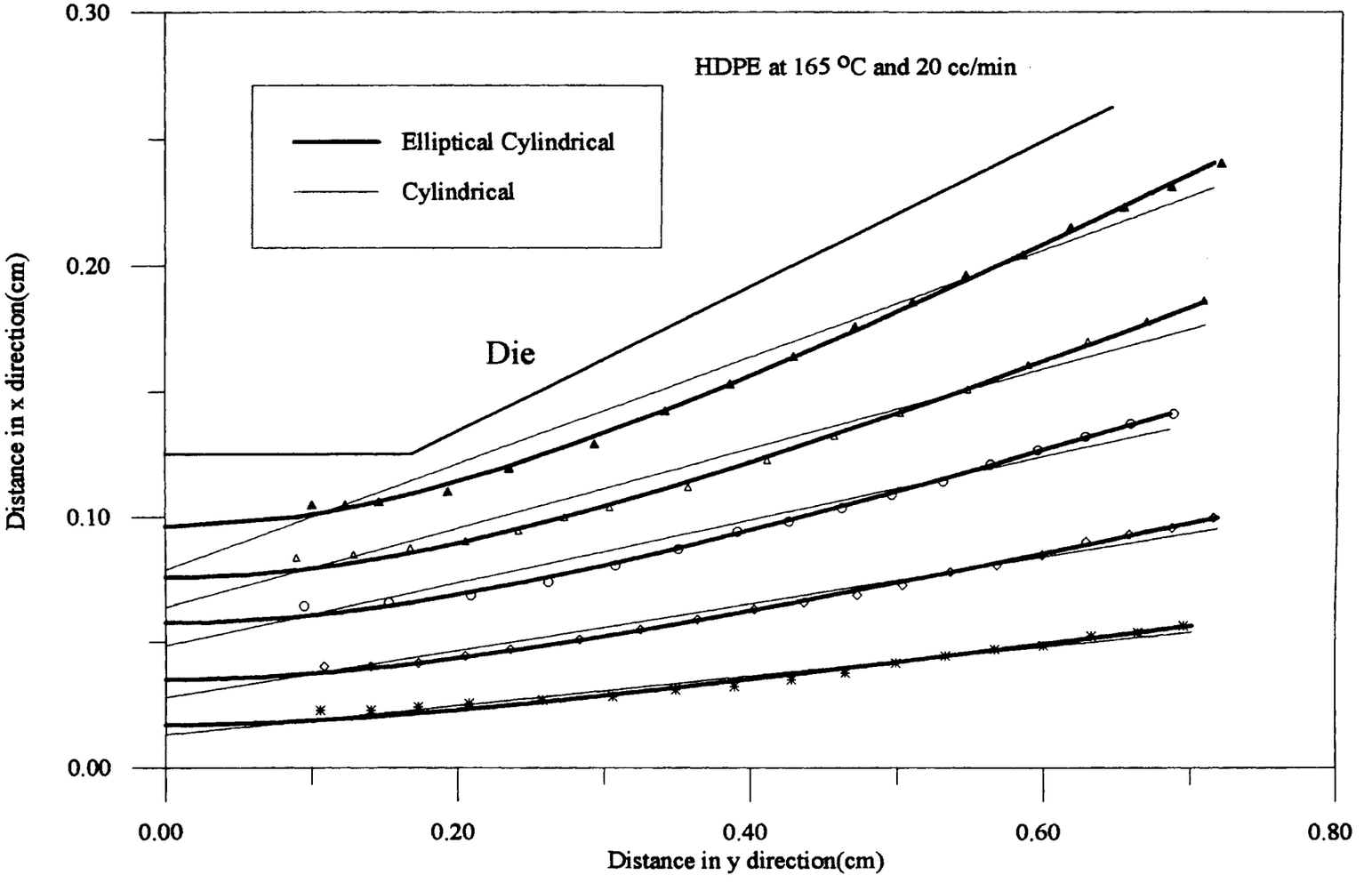

Fig 4.4 : Comparision Between Elliptic Cylindrical and Cylindrical Coordinates

representation of the path traced by the particles irrespective of temperature, flow rate and material than are the paths in cylindrical coordinates.

The observations made in this chapter clearly demonstrate that working in elliptical cylindrical coordinates allows a more accurate representations of the streamlines.

4.2 Elliptical Cylindrical Coordinate System

In order to work in any coordinate system, the equations of motion and continuity in that coordinate system are essential. Since the elliptical cylindrical coordinate system is not in common usage, the equations of motion and continuity were not readily available. In this section, the different equations required to work in the elliptical cylindrical coordinate system are derived from the equations of motion and continuity for general orthogonal coordinates. The general equation of motion is given as

$$\frac{\partial}{\partial t}\rho v = -[\nabla\cdot\rho vv]-[\nabla\cdot\pi]+\rho g \tag{4.1}$$

and the equation of continuity is given as

$$\frac{\partial \rho}{\partial t} = -(\nabla\cdot\rho v). \tag{4.2}$$

Where ρ = density,

v = velocity,

g = acceleration due to gravity,

π = stress tensor,

∇ = gradient operator.

In general orthogonal coordinates, the gradient operator is given as

$$\nabla = \sum_{\alpha} \frac{\delta_\alpha}{h_\alpha} \frac{\partial}{\partial q_\alpha} \tag{4.3}$$

where δ_α = unit vectors

h_α = scale factors

q_α = orthogonal coordinates

The scale factors for the elliptic cylindrical coordinate system were derived in Appendix B and are

$$h_\psi^2 = a^2(\sinh^2\psi + \sin^2\eta) = h_\eta^2, \qquad h_z = 0. \tag{4.4}$$

Scale factors are characteristic of a coordinate system and arise when the unit vectors in rectangular coordinate system are converted to unit vectors in the coordinate system of interest.

For polymeric materials constant density may be assumed, and Eq. 4.2 simplifies to:

$$(\nabla \cdot v) = 0. \tag{4.5}$$

Combining Eqs. 4.3 to 4.5, the continuity equation was found to be

$$\frac{1}{h^2}\frac{\partial(hv_\psi)}{\partial\psi} + \frac{1}{h^2}\frac{\partial(hv_\eta)}{\partial\eta} + \frac{\partial v_z}{\partial z} = 0. \tag{4.6}$$

Combining Eqs. 4.1 with 4.3 through 4.4 the equations of motion were found to be

$$\rho\left(\frac{\partial v_\psi}{\partial t}+\frac{v_\psi}{h}\frac{\partial v_\psi}{\partial \psi}+\frac{v_\eta}{h}\frac{\partial v_\psi}{\partial \eta}+v_z\frac{\partial v_\psi}{\partial z}+\frac{A}{h}v_\psi v_\eta-\frac{B}{h}v_\psi v_\psi\right)$$

$$=-\left(\frac{1}{h^2}\frac{\partial}{\partial \psi}(h\tau_{\psi\psi})+\frac{1}{h^2}\frac{\partial}{\partial \eta}(h\tau_{\eta\psi})+\frac{\partial}{\partial z}(\tau_{z\psi})+\frac{A}{h}\tau_{\psi\eta}-\frac{B}{h}\tau_{\eta\eta}\right) \tag{4.7a}$$

$$+\rho g_\psi-\frac{1}{h}\frac{\partial P}{\partial \psi},$$

$$\rho\left(\frac{\partial v_\eta}{\partial t}+\frac{v_\psi}{h}\frac{\partial v_\eta}{\partial \psi}+\frac{v_\eta}{h}\frac{\partial v_\eta}{\partial \eta}+v_z\frac{\partial v_\eta}{\partial z}+\frac{A}{h}v_\eta v_\eta-\frac{B}{h}v_\psi v_\psi\right)$$

$$=-\left(\frac{1}{h^2}\frac{\partial}{\partial \psi}(h\tau_{\psi\eta})+\frac{1}{h^2}\frac{\partial}{\partial \eta}(h\tau_{\eta\eta})+\frac{\partial}{\partial z}(\tau_{z\eta})-\frac{A}{h}\tau_{\psi\psi}+\frac{B}{h}\tau_{\eta\psi}\right) \tag{4.7b}$$

$$+\rho g_\eta-\frac{1}{h}\frac{\partial P}{\partial \eta}$$

$$\rho\left(\frac{\partial v_z}{\partial t}+\frac{v_\psi}{h}\frac{\partial v_z}{\partial \psi}+\frac{v_\eta}{h}\frac{\partial v_z}{\partial \eta}+v_z\frac{\partial v_z}{\partial z}\right)$$

$$=-\left(\frac{1}{h^2}\frac{\partial}{\partial \psi}(h\tau_{\psi z})+\frac{1}{h^2}\frac{\partial}{\partial \eta}(h\tau_{\eta z})+\frac{\partial}{\partial z}(\tau_{zz})\right) \tag{4.7c}$$

$$+\rho g_z-\frac{\partial P}{\partial z},$$

where

$$h=h_{\psi} = h_{\eta},$$
$$A = \frac{1}{h}\frac{\partial h}{\partial \eta} \qquad B = \frac{1}{h}\frac{\partial h}{\partial \psi}. \tag{4.8}$$

Eqs. 4.6 to 4.8 are essential for working in the elliptical cylindrical coordinate system. Once these equations were obtained, the appropriate assumptions of the specific system under consideration can be applied to arrive at simpler equations. Eqs. 4.7 and 4.8 can then be solved simultaneously, applying the boundary conditions of the system, to arrive at velocity fields. The velocity fields can then be used to arrive at the flow kinematics. Also, the number of equations to be solved can be reduced by the stream function method. Flow kinematics can also be obtained from the experimental velocity fields. The next two sections give the calculation of the flow kinematics in elliptical cylindrical coordinates under the assumption of a Newtonian fluid and from the experimental data.

4.3 Theoretical Analysis

The aim of this analysis is to arrive at an equation for the velocity fields, given the volumetric flow rate and the converging angle for the channel. This procedure requires the assumption of a particular rheological equation of state.

The converging channel in this study can be represented as shown in Figure 4.5 in elliptical cylindrical coordinates. The streamlines are lines of constant η with varying ψ. The edge of the die can be approximated as a line of constant η as shown. In the converging channel, the velocity field is given by

$$v_\psi = v_\psi(\psi,\eta) \quad , \quad v_\eta = v_z = 0. \tag{4.9}$$

Substituting Eq. 4.9 into the continuity equation Eq. 4.6 gives,

$$\frac{\partial}{\partial\psi}(hv_\psi) = 0. \tag{4.10}$$

Rearranging Eq. 4.10 gives

$$v_\psi(\psi,\eta) = \frac{f(\eta)}{h}, \tag{4.11}$$

in which $f(\eta)$ is a function dependent on η only. The function $f(\eta)$ will be determined when the equations of motion are solved for $v_\psi(\psi,\eta)$ subject to the boundary

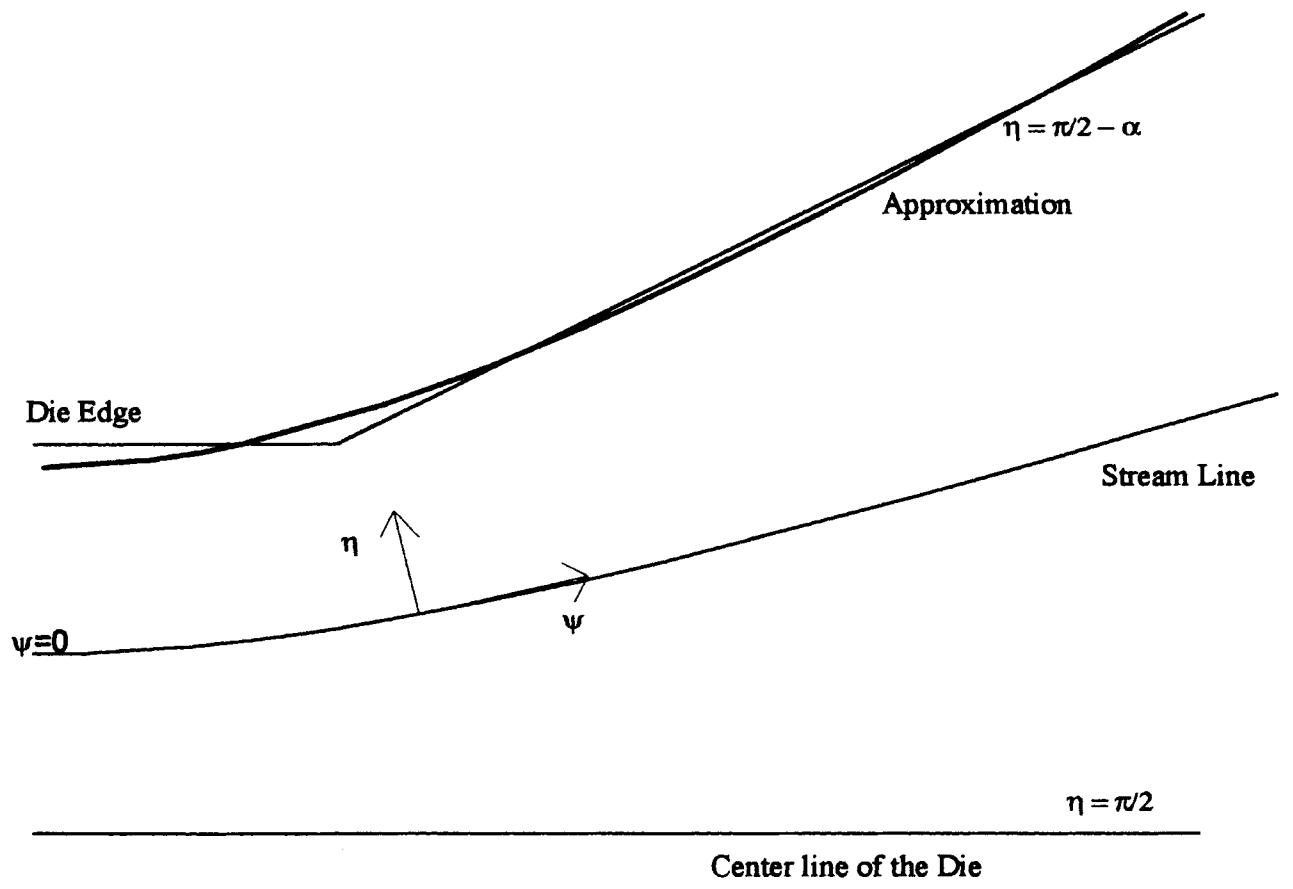

Fig 4.5 : Representation of the Converging Channel in Elliptical Cylindrical Coordinates

conditions specified as

$$v_{\psi}(\psi,\eta = \frac{n\pi}{2}\pm\alpha) = 0, \tag{4.12a}$$

$$\left(\frac{\partial v_{\psi}}{\partial \eta}\right)_{\eta=\frac{n\pi}{2}} = 0, \tag{4.12b}$$

which can be rewritten as

$$\begin{aligned} f(\frac{n\pi}{2}\pm\alpha) &= 0, \\ f'(\frac{n\pi}{2}) &= 0, \end{aligned} \tag{4.13}$$

where n is an odd number and a prime indicates differentiation w.r.t η.
The $f(\eta)$ term thus obtained will contain the f(0) term which has to be determined from the volumetric flow rate per unit length of the channel width. This solution of $f(\eta)$ for the velocity fields can be used for any converging channel once the volumetric flow rate and the converging angle are known. Once the velocity fields are known the components of the rate of strain tensor can be calculated.

The equation of motion in elliptical cylindrical coordinates for the velocity fields described in Eq. 4.9 can be written as

$$\left(\frac{1}{h^2}\frac{\partial}{\partial\psi}(h\tau_{\psi\psi})+\frac{1}{h^2}\frac{\partial}{\partial\eta}(h\tau_{\eta\psi})+\frac{A}{h}\tau_{\psi\eta}-\frac{B}{h}\tau_{\eta\eta}+\frac{1}{h}\frac{\partial P}{\partial\psi}\right) = 0 \tag{4.14a}$$

$$\left(\frac{1}{h^2}\frac{\partial}{\partial\psi}(h\tau_{\psi\eta})+\frac{1}{h^2}\frac{\partial}{\partial\eta}(h\tau_{\eta\eta})-\frac{A}{h}\tau_{\psi\psi}+\frac{B}{h}\tau_{\eta\psi}+\frac{1}{h}\frac{\partial P}{\partial\eta}\right) = 0, \tag{4.14b}$$

when the inertial terms involved are neglected which is justifiable for the very viscous polymer melts considered.

Solving Eq. 4.14 requires a relationship between the components of stress and deformation rate. The use of rheological models of the integral type would be desirable for this type of flow. However, before applying a higher order model, the solution procedure will be checked for a simple model like the Newtonian fluid. The Newtonian model can be represented as

$$\tau_{ij} = \mu\dot{\gamma}_{ij}, \tag{4.15}$$

where

$$\dot{\gamma}_{ij} = \{\nabla v\}_{ij}+\{\nabla v\}_{ji}. \tag{4.16}$$

The $\{\nabla v\}$ operators for the elliptical cylindrical coordinates were derived using the procedure given in Bird (Bird, 1987) and are listed in the Appendix C.

Using the operators given in Appendix C and substituting Eq. 4.11 into Eq. 4.15

results in

$$\tau_{\psi\psi} = \frac{2\mu Bf}{h^2}, \tag{4.17a}$$

$$\tau_{\eta\eta} = -\frac{2\mu Bf}{h^2}, \tag{4.17b}$$

$$\tau_{\psi\eta} = \tau_{\eta\psi} = -\frac{\mu}{h^2}(f'-2Af). \tag{4.17c}$$

Substitution of Eqs. 4.17 into Eq. 4.14 and using the condition that

$$\frac{\partial h}{\partial \eta} \ll \frac{\partial h}{\partial \psi}, \tag{4.18}$$

we have

$$\frac{\partial P}{\partial \eta} = \frac{2\mu Bf'}{h^2} \tag{4.19}$$

$$\frac{\partial P}{\partial \psi} = -\mu\left(\frac{2f}{h^2}\frac{\partial B}{\partial \psi} - \frac{f''}{h^2}\right). \tag{4.20}$$

Eq. 4.18 was arrived at by testing the equation at different values of η and ψ.

The pressure terms can be eliminated from Eqs. 4.18 and Eq. 4.20 by differentiating Eq. 4.18 with respect to Ψ and Eq. 4.20 with respect to η. Combining the resulting expressions gives

$$f'''+4f'(B^2-\frac{\partial B}{\partial \psi}) = 0. \tag{4.21}$$

Eq. 4.21 has to be solved subject to the boundary conditions in Eq. 4.13. No analytical solution was found for this equation. If a higher order rheological model is employed, the equation to be solved would be much more complicated and would require a more rigorous approach of solution.

4.4 Stream Function

The stream function is an important analytical tool for the solution of flow problems. Here the velocity components are expressed in terms of Ψ in such a way that the continuity equation is automatically satisfied. The physical significance of a stream function is that the lines of constant Ψ are stream lines.

In the case of the elliptical cylindrical coordinate system for the converging channel shown in Figure 4.5, the velocity components are

$$v_{\psi} = \frac{\Psi(\eta)}{h}, \tag{4.22a}$$

and

$$v_{\eta} = 0 \ , \ v_{z} = 0. \tag{4.22b}$$

The equation of continuity was automatically satisfied by the above representation of velocity components. Eq. 4.22 is essentially same as Eq. 4.11. The functionality of the stream function can be found from the tracer particle data. In elliptical cylindrical coordinates for this flow geometry the stream lines are lines of constant η. As Ψ is a function of η only, the stream lines are also the lines of constant Ψ, which is consistent with the definition of stream function. For a stream line, the v_{ψ} at any ψ can be calculated. Using these values, the value of Ψ for the stream line can be calculated by the method of least squares from Eq. 4.22a. In a similar way the value

of Ψ for all the stream lines can be calculated and plotted against η to give the functionality of Ψ. Once the exact functionality of the stream function is known, the rate of strain tensor can be calculated from the equation

$$\dot{\gamma}_{ij} = \{\nabla v\}_{ij} + \{\nabla v\}_{ji}. \tag{4.23}$$

Substituting Eq. 4.22 in Eq. 4.23 yields

$$\dot{\gamma}_{\psi\psi} = -\dot{\gamma}_{\eta\eta} = \frac{\Psi c \sinh(2\psi)}{h^4}, \tag{4.24}$$

and

$$\dot{\gamma}_{\psi\eta} = \frac{\Psi_\eta}{h^2} - \frac{\Psi c Sin(2\eta)}{h^4}. \tag{4.25}$$

In this section, results of the converging channel kinematics are presented for the case of LLDPE at 165 °C and 16 cc/min. This material and flow conditions were selected as an example because it represented a well behaved material at very modest flow rates and a typical processing temperature for the material.

The value of η was calculated for every stream line in Figure 4.1 using Eq. 3.1 and 3.2. The x and y coordinates from each point were used to calculate the value of ψ at that point for the entire stream line. The value of v_ψ at each point was then calculated using the method of finite difference. From these values of v_ψ the value of $\Psi(\eta)$ was calculated by the method of least squares from Eq. 4.22a. The

values of Ψ as a function of η for 7 tracer particles is shown in Table 4.1.

The data from Table 4.1 was fit to a polynomial of degree 2 and is shown in Figure 4.6. The functionality was found to be

$$\Psi(\eta) = -3.246+4.476\eta-1.47\eta^2 \tag{4.26a}$$

$$\Psi_\eta(\eta) = 4.476-2.94\eta. \tag{4.26b}$$

Where η is in rad, Ψ is in cm^2/sec^{-1} and Ψ_η is in cm^2/sec^{-1}. From Eqs. 4.26a and 4.26b the elements of the rate of strain tensor could be calculated from Eq. 4.24 and Eq. 4.25, and are shown in Section 4.8. Similar calculations of the functionality of Ψ was carried out for different flow rates and materials like HDPE and are shown in Appendix F.

Converging Channel Kinematics

Ψ, cm^2/sec^{-1}	η, Rad
0.1559	1.500
0.1507	1.443
0.1365	1.397
0.1212	1.362
0.0970	1.319
0.0675	1.279
0.0531	1.250

Table 4.1 :Values of Ψ as a Function of η for LLDPE at 165 °C and 16 cc/min

4.5 Stress Optic Data

Birefringence data was collected and analyzed for LLDPE and HDPE at different temperatures and flow rates. When the polarizer and the analyzer were crossed and there is no flow in the channel no birefringence was observed, and the field was dark. When the flow of the polymer was started, by switching on the screw, alternating dark and bright bands originated from the upper and lower walls of the slit, and approached the center. As the flow became steady, the appearance of new bands stopped and the position of the bands remained constant. These bands are called the isochromatics. The dark band left over from the dark field at the beginning of the flow, is known as the zero order band. The first dark band originating from the walls assumed a position near the center of the channel. This band is known as the first order band. The bands above and below the zero order band were given the order of first, second, third, etc. An example of the birefringence pattern in the converging section is shown in the Figure 4.7 for the case of LLDPE at 160 °C and 12 cc/min and $\alpha=0$. The number and position of isochromatics are strongly dependent on the flow rate. As flow rate of the polymer melt increased the number of dark and bright bands increased. These isochromatic bands correspond to the locus of points with constant principal stress difference.

As the polarizer and the analyzer were rotated in unison in the counter clockwise direction, the dark bands or the isochromatics, moved down and a dark band appeared at the upper edge of the converging channel. At the same time the

Figure 4.7: Birefringence Patterns in the Converging Channel

band closest to the lower edge of the channel started to disappear. When $\alpha=90°$ each dark band attained the position previously occupied by dark bands below. This behavior is documented in Figure 4.8. The points in the Figure 4.8 denote the position of the center of the dark bands for different α. The error bars used were an approximate errors in calculating the position of band. This behavior was different from the observation of the previous experimenters (Han & Drexler, 1973a; Han & Drexler, 1973b; Han & Drexler, 1973c; Yoo & Han, 1981) and is inconsistent with Eq. 2.12. Eq. 2.12 suggests that isochromatics will not change positions. The same behavior was observed at different flow conditions and temperature and with different materials.

When the birefringence was observed in the slit flow section the isochromatics were found to be stationary. Figure 4.9 shows the position of the center of the dark bands for different α. Therefore in the slitflow section the isochromatics agree with Eq. 2.12.

The following reasons for the shifting of the isochromatic bands in the converging section have been investigated:

(i) The polarizer and the analyzer may have been damaged: This hypothesis was checked by setting up the optical train without the sample in between the polarizer and the analyzer and the camera replaced by a cathetometer. The polarizer and the analyzer were crossed and the cathetometer was focused on the analyzer. When viewed through the cathetometer if there were spots of bright light leaking through then it could be concluded that the polarizers were damaged. Since there were no

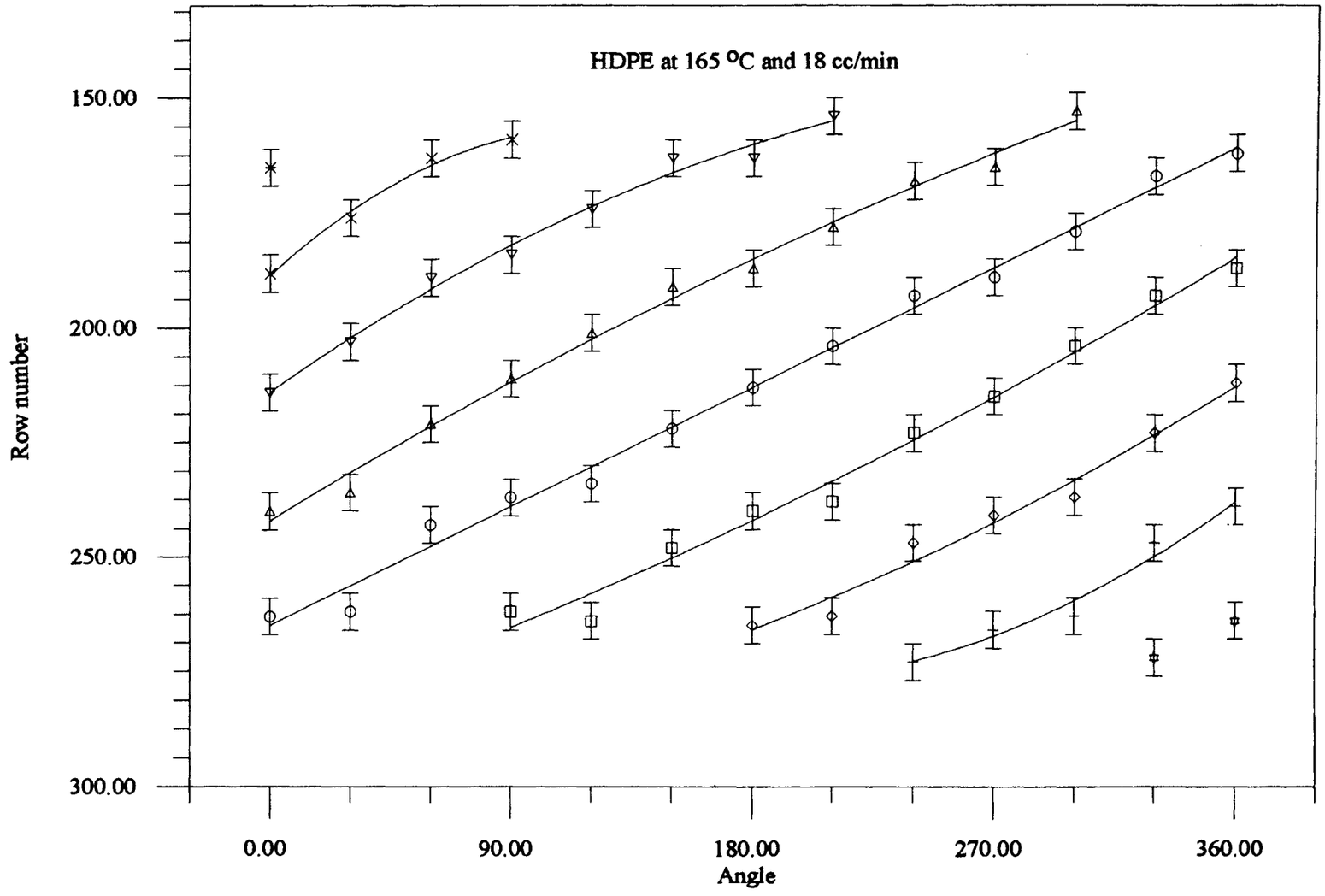

Fig 4.8: Position of the Isochromatics Bands at the Slit Flow Entrance of the Converging Channel

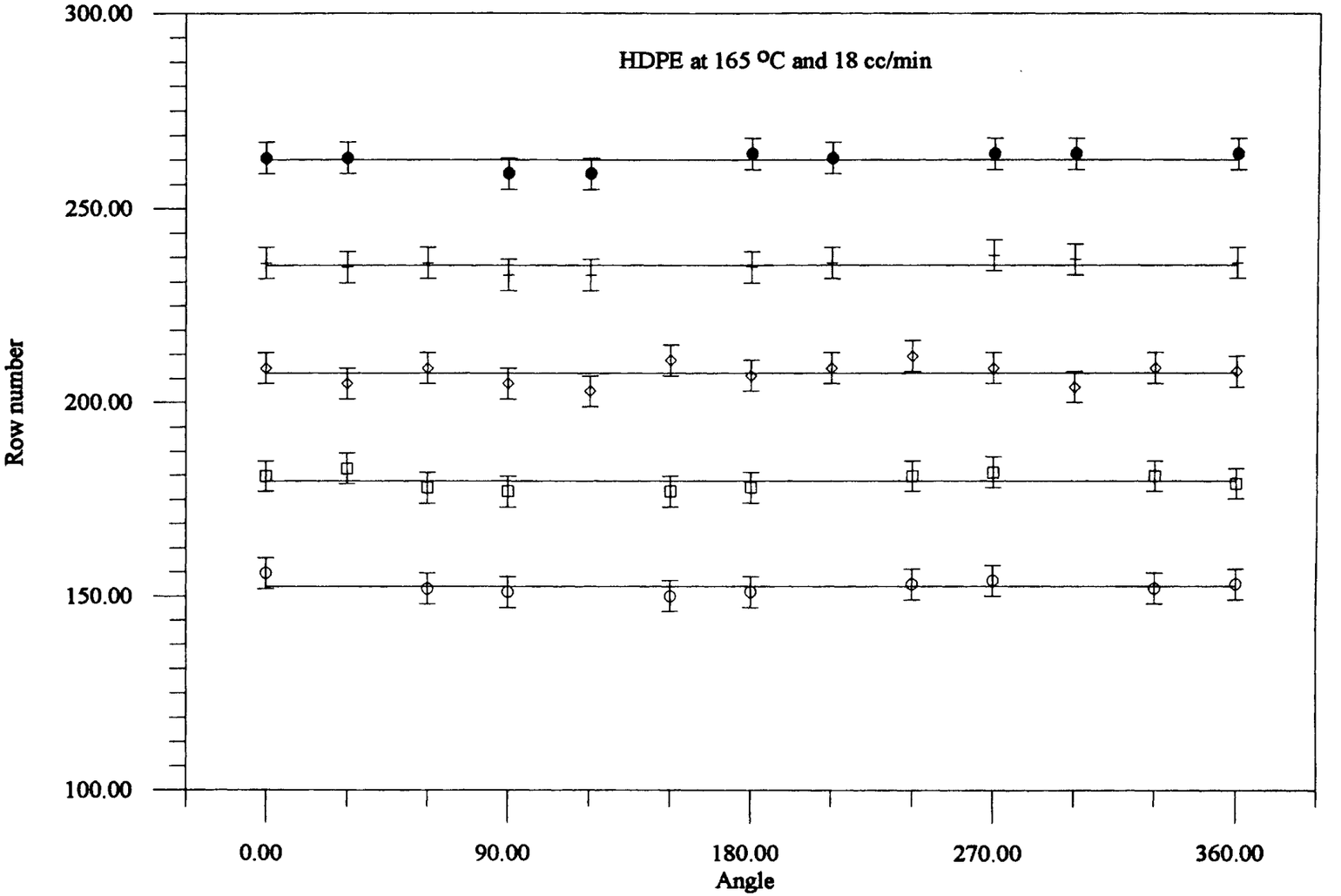

Fig 4.9 : Position of the Isochromatics Bands in the Slit Flow Section

Here n'' is the imaginary part of the refractive index in the equation

$$\underline{n} = \underline{n}'+i\underline{n}''. \tag{4.30}$$

From the Eq. 4.27 demonstrate that dark bands due to dichroism appear only when either $\cosh\kappa$ is equal to $\cos\delta$ which can only be possible when $\cosh\kappa=1$, since $\cosh\kappa$ varies from 1 to ∞ and $\cos\delta$ varies from 0 to 1. This suggests that only one dark band other than the isoclinics can appear. However the birefringence studies show that there is more than one dark band, other than the isoclinic present. Therefore Eq. 4.27 could not explain the occurrence of multiple isochromatic bands, which leads to the conclusion that dichroism is not significant.

(iii) Wall effects: In order to get the stress distribution of polymer flow in the converging channel using measurements of flow birefringence, there should be no variations in optical properties along the optical path i.e. the flow field must be two dimensional. In the converging channel used in this study the flow was not perfectly two-dimensional. In order to consider the flow as two-dimensional the experimental geometry must have a sufficiently high aspect ratio. Aspect ratio is the ratio of breadth of the channel to height of the channel. The optimum aspect ratio was suggested by Janeschitz-Kriegl (Janeschitz-Kriegl, 1983) to be 10. Janeschitz-Kriegl also suggested a optimum optical pathlength which does not exceed 100 mm. The aspect ratio in the converging channel varies from 10 at the slit flow entrance to a minimum of 5 in the converging section and the optical path length is less than 100 mm. This does not satisfy fully the practical experimental considerations for a two-

dimensional flow. To test the assumption of two dimensionality of the flow, the camera was focussed on 9 eqi-distant planes with a distance between each plane of 0.125 inches. The tracer particles exactly on the center line of the converging channel (i.e. x=0) for each plane were analyzed and the velocity change with distance in the y direction was determined. Figure 4.10 gives a plot of velocities as function of distance in z direction for different planes of focus for HDPE at 165°C and 13 cc/min in the converging section. Figure 4.11 gives a similar plot in the entrance region. From the Figures 4.10 and 4.11 large velocity deviations can be seen within a small distance from the wall, leading to a plug flow like profile over most of the channel. This flow can be considered as a two dimensional core flanked by stress boundary layers near the walls. Similar flow conditions have been studied by Burghardt & Fuller, Galante & Frattini and McHugh, et al. (Burghardt & Fuller, 1989; Galante & Frattini, 1991; McHugh, Mackay, & Khomami, 1987). Galante and Frattini (Galante & Frattini, 1991) have shown that the stress boundary layers are nearly isotropic in the direction of the optical path, and thus have negligible influence on the polarization state of light propagating through them. McHugh and Galante showed that these layers only caused an isoclinic band spreading and did not decrease with an increase in the aspect ratio of the channel. Therefore it can be concluded that the movement of the isochromatics could not have been due to the wall effects.

(iv) The light used is not purely monochromatic: Eq. 2.12 demands that a monochromatic light source be used to observe isochromatics clearly. The filter used to obtain monochromatic light is an bandpass interference filter with a center wave

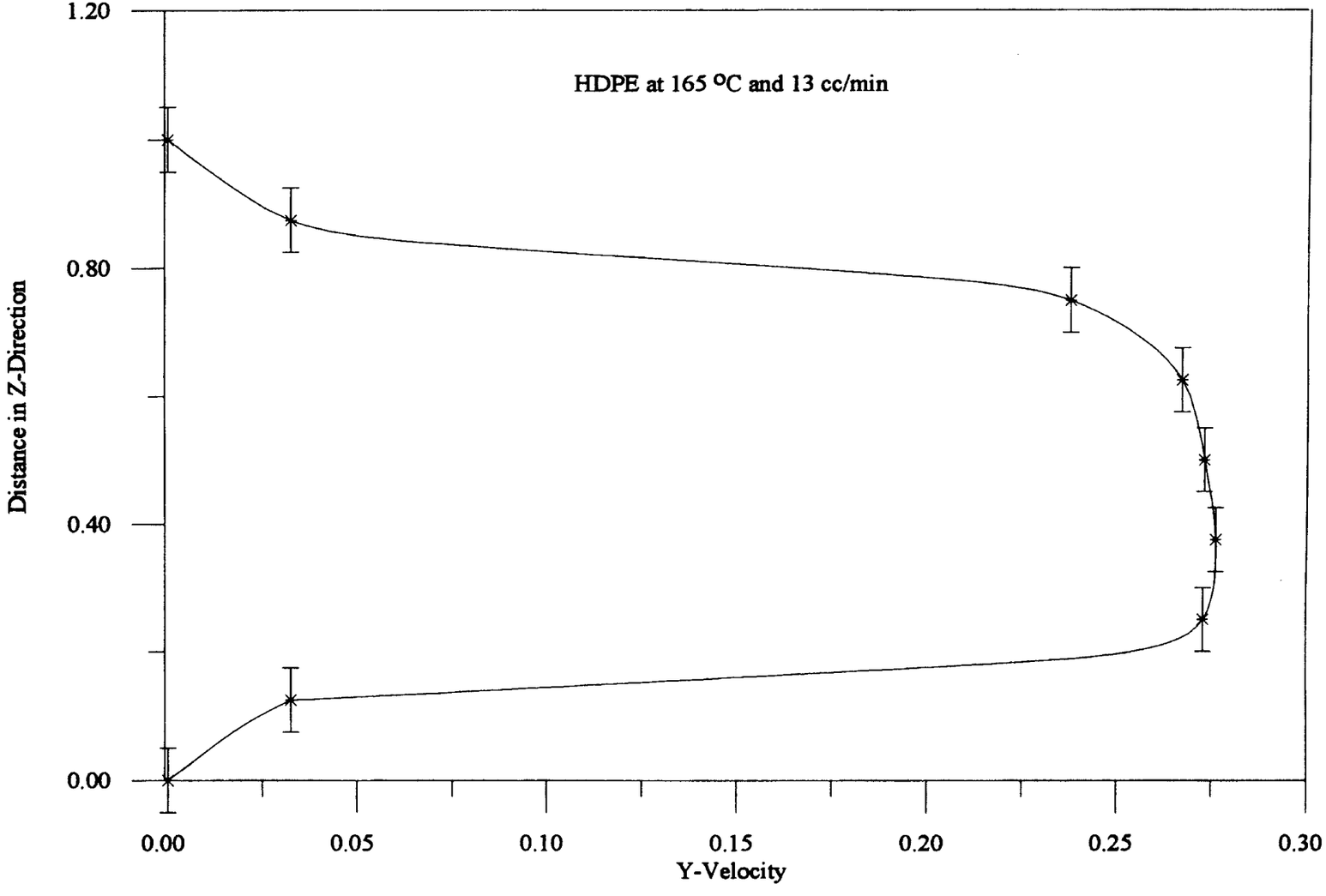

Fig 4.10: Velocity Profile in Z-Direction In the Converging Channel

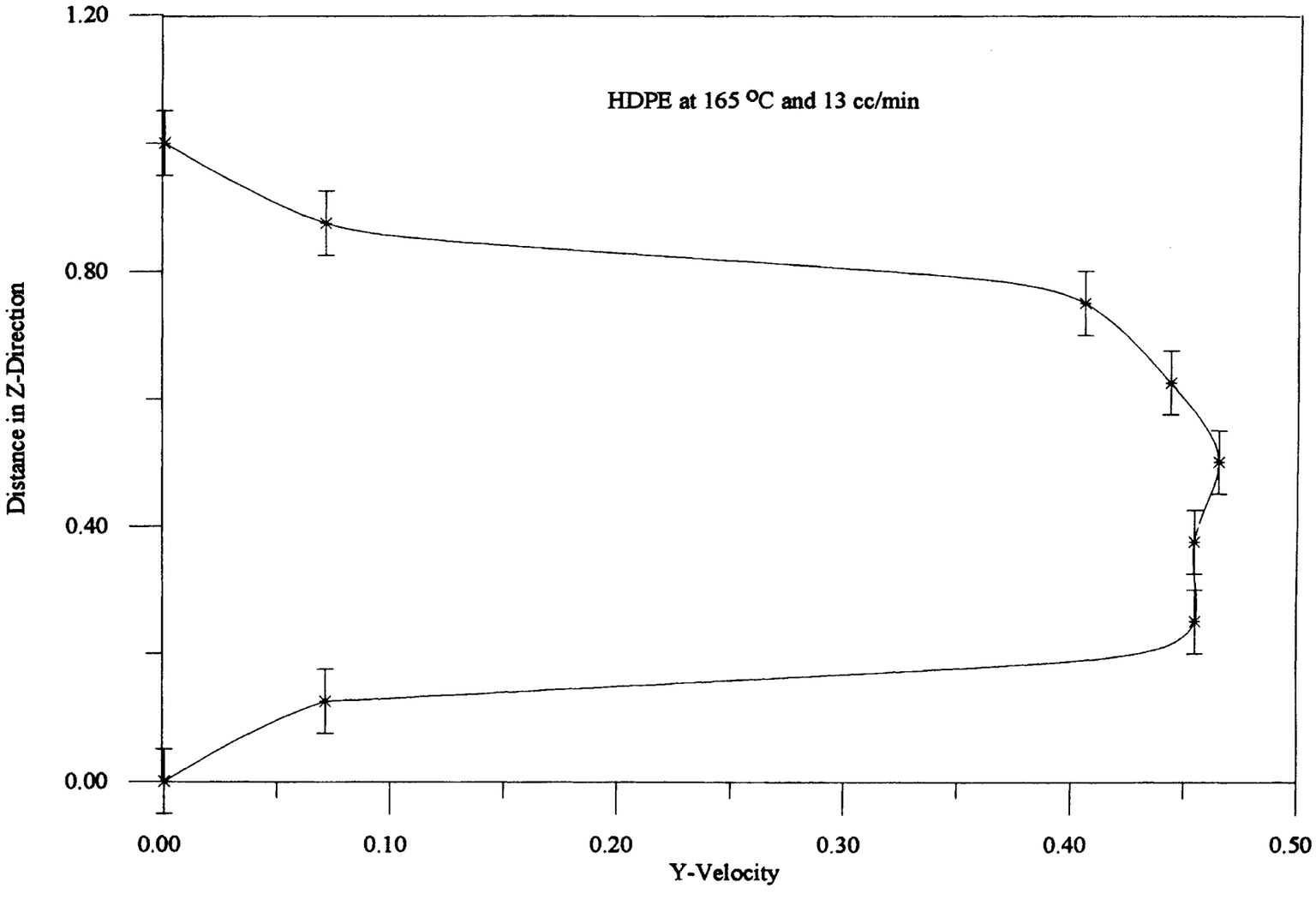

Fig. 4.11: Velocity Profile in z-direction at the Entrance of the Channel

length of 488 nm and a band width of 7.2 nm. So the light used is not purely monochromatic and might be the reason for the deviations.

(v) The wavelength of the light used is not appropriate: Han, Drexler and Park, et al. (Han & Drexler, 1973c; Park, Kiriakidis, & Mitsoulis, 1992) and other researchers working on flow birefringence have used a green monochromatic interference filter with a center wave length of 546.1 nm. Larson, et al., McHugh et al.,and Rajagopalan et al. (Larson, Khan, & Raju, 1988; McHugh, Mackay, & Khomami, 1987; Rajagopalan, Byars, Armstrong, & Brown, 1992) used a 559.8 nm light for their flow birefringence experiments. No reasons have been given as to why the particular wavelength of light was used in their studies. The wavelength of the light used in this study was 488 nm and was different from that used by researchers before and might be the reason for the observations.

(vi) The thickness of the channel (in the Z-direction) is varying: The thickness of the channel in the direction of the light propagation may be changing due to expansion upon heating or due to the increased pressure at higher flow rates. Eq. 2.12 shows that this variation of thickness, L, will cause a shift in the isochromatics. But the movement of the isochromatics with the change in orientation angle of polarizer cannot be explained with this hypothesis.

(vii) The optical train used is different from the one used by other researchers: Han, Drexler, McHugh, Et al., and Rajagopalan, et al. (Han & Drexler, 1973b, McHugh, Mackay, & Khomami, 1987; Rajagopalan, Byars, Armstrong, & Brown, 1992) used an opal plexiglass in the optical train to diffuse the light and make it more

uniform. In this study nothing was used to diffuse the light. Since the same optical train was used in the slit flow section this hypothesis can be ruled out.

(viii) Material properties: The same behavior was observed in different materials like HDPE and LLDPE. Therefore material dependency can be ruled out.

In addition, the birefringence studies were carried out using white light. Han, Drexler and Park, et al. (Han & Drexler, 1973c; Park, Kiriakidis, & Mitsoulis, 1992) have used white light to clearly identify the isoclinic which appears as dark band against the multi colored isochromatics. The optical setup described in Chapter 3 was modified by removing the monochromatic filter to allow white light to pass through the optical train. The birefringence data was recorded for every 10° change in the polarizer-analyzer angle. The birefringence patters for HDPE at 165 °C and 20 cc/min are presented in Figure 4.12.

In Figure 4.12 the birefringence patterns are presented for polarizer/analyzer angles of 0°, 10°, 20°, 30°, 40° and 45°. In the picture in Figure 4.12a there is a dark band at the center of the channel flanked by two colored bands on either side. The dark band at the center of the channel moves up as the polarizer and the analyzer are rotated in the counter clockwise direction and disappears when α is 45^0. This can be considered to be an isoclinic band. The other bands do not move with the change in α and can be considered the isochromatics. The same phenomenon was observed in HDPE at a higher flow rate and the same temperature. Therefore it can be safely assumed that the dark band at the center of the channel is the isoclinic band. The stress fields can be now calculated using Eqs. 2.10-2.11 and the stress optic

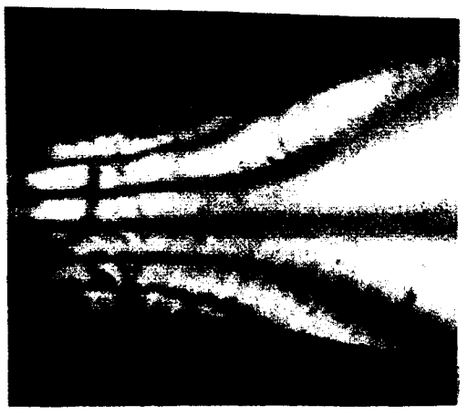

(a)

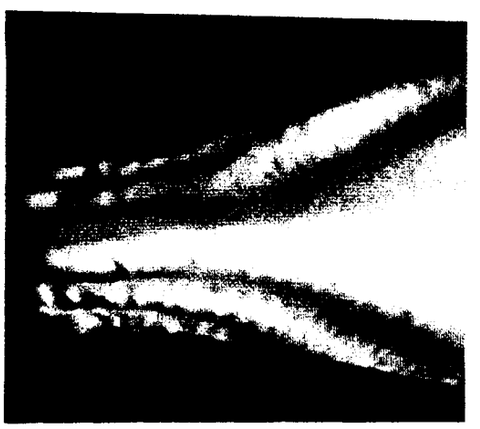

(b)

(c)

Figure 4.12: Full Color Birefringence Patterns in the Converging Channel for HDPE at 165 °C and 20 cc/min and α = 0° to 20°, a) α = 0° b) α = 10° c) α = 20°.

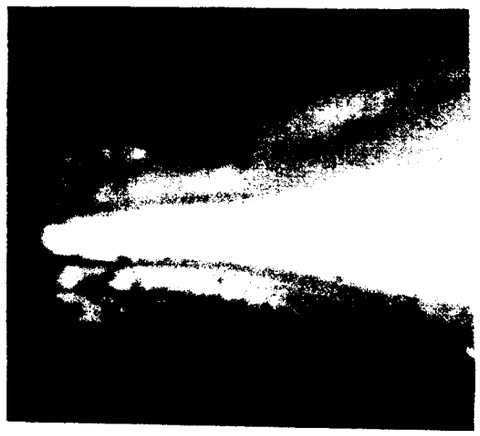

(d)

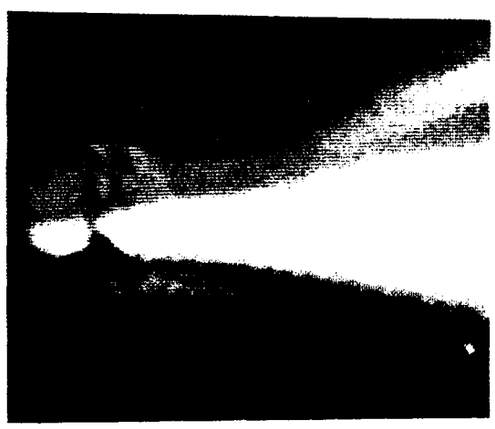

(e)

(f)

Figure 4.12: Full Color Birefringence Patterns in the Converging Channel for HDPE at 165 °C and 20 cc/min and α = 30° to 45°, d) α = 30° e) α = 40° f) α = 45°.

coefficient. The χ and Δn at any point were calculated by interpolation from the isochromatics and the isoclinics contours. The isochromatic and the isoclinic contours were traced as described in section 3.3 using the image processing software IRIS-T.

The isochromatic and the isoclinic contours for HDPE at 165 °C and 20 cc/min are shown in figures 4.13 and 4.14. The order of the isochromatic bands was determined by looking at the birefringence at the start of the flow. The bands are numbered in the order of appearance as the flow started and became steady. The dark bands are numbered as 0, 1 ,2 and the bright bands as 0.5, 1.5, 2.5. When the value of the argument of the sin term in Eq. 2.12 is a integral multiple of π there is a dark band and when it is the integral multiple of $\pi/2$ there is a white band. But the zero order band could not be located after the flow became steady. This observation can be explained by suggesting that the zero order band has moved downstream into the slit flow section of the converging channel and could not be seen in the field of vision. This hypothesis was arrived at by observing the birefringence patterns obtained by Han and Drexler (Han & Drexler, 1973b) in a converging channel, where the field of vision was greater than the one in this study.

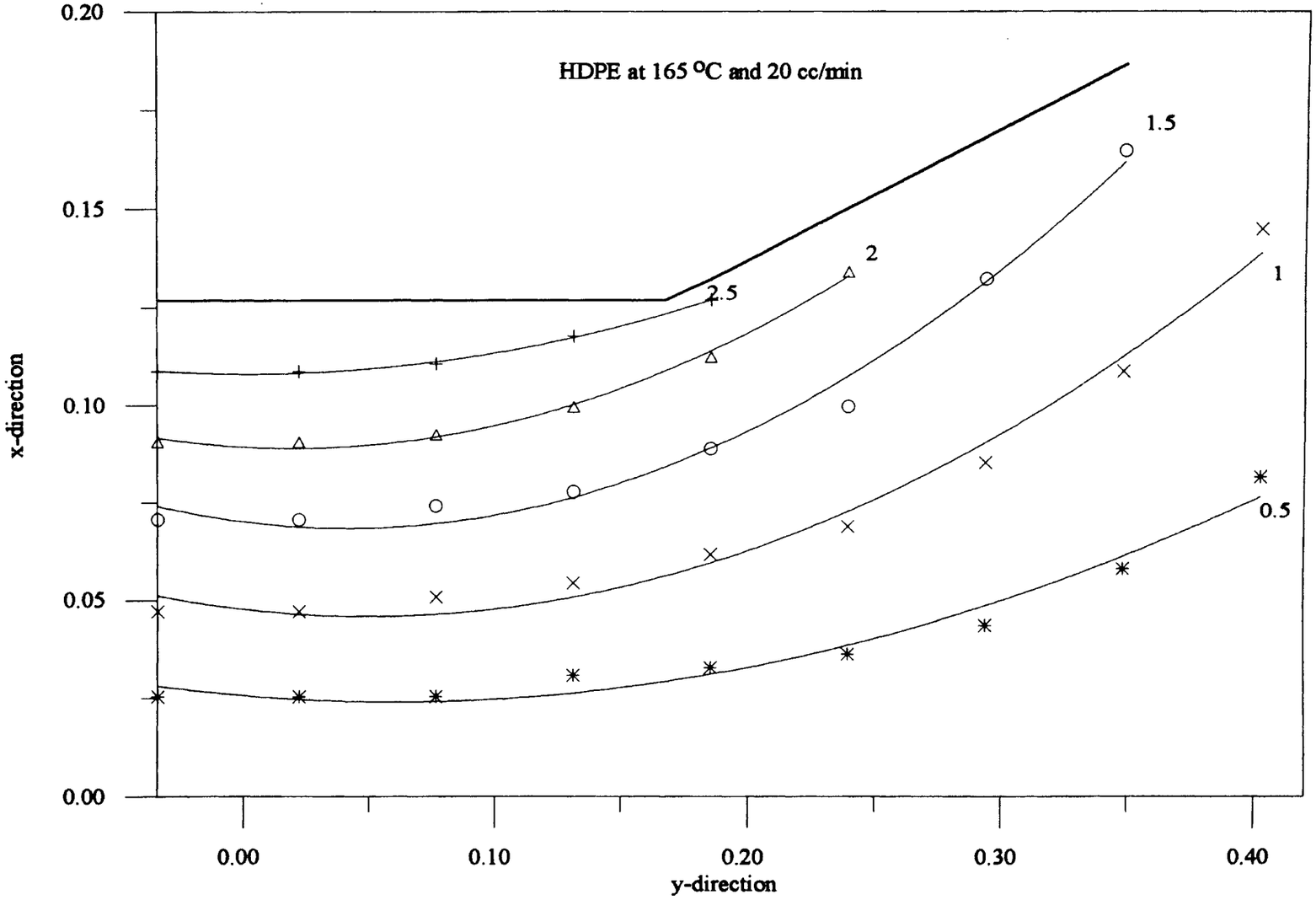

Fig 4.13 : Isochromatic Contours in the Converging Channel

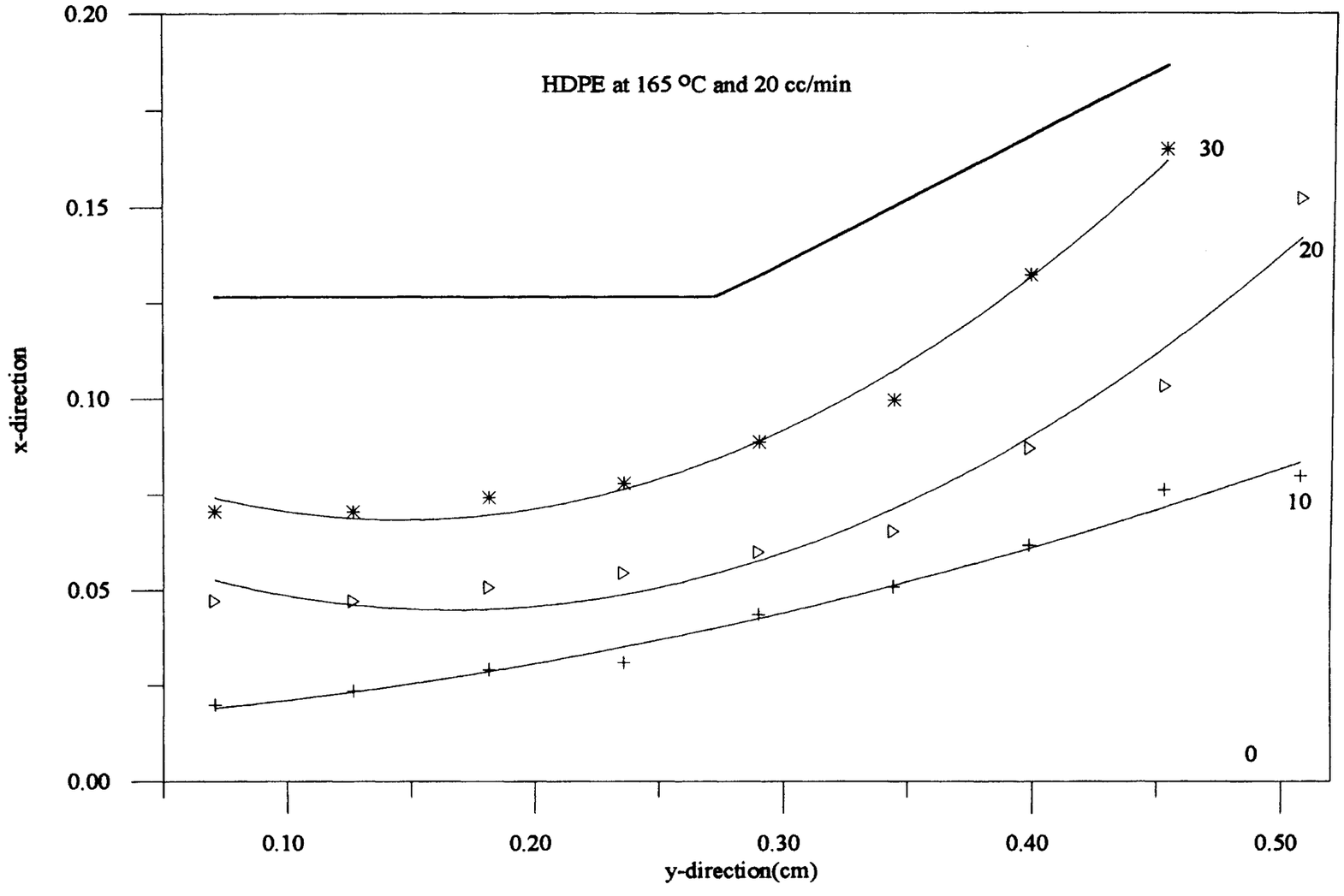

Fig 4.14: Isoclinic Contours in the Converging Channel

4.6 Stress Optic Coefficient

The stress optic coefficient can be measured using the Method of Isoclinics (Janeschitz-Kriegl, 1983). In the slit section where the flow is fully developed and the pressure drop is known, the position of the isochromatics and the isoclinics were determined by rotating the polarizer and analyzer. The stress optic coefficient for HDPE at 165 °C is calculated in this section. The pressure gradient for this case was 13.57 x 10^6 N/m^2. As suggested by McHugh, Mackay, and Khomami (McHugh, Mackay, & Khomami, 1987), the inside edge of the isoclinic closest to the center of the flow is considered to be the point where the value of χ is equal to the angle of rotation. The value of χ at five such points were found at rotation angles of 35, 40, 45, 50, 55. Δn at these points was calculated by interpolation from the values obtained at the positions of isochromatics. The value of shear stress at each point was calculated using the following equation:

$$\tau_{xy} = y\frac{\partial P}{\partial x}, \tag{4.31}$$

where x = distance in the direction of flow,

y = the position of isoclinic relative to the center of flow,

τ_{xy} = Shear stress

P = pressure.

The shear stress was plotted as a function of $(\Delta/2)\sin(2\chi)$ as per Eq. 2.10 and is

shown in Figure 4.15. The line is a least squares fit to the data passing through the origin. The data points fall on or near the line indicating the validity of the stress optic relationship. The inverse of the slope of the line is the stress optic coefficient. From Figure 4.15, C= 1.46 X 10^{-9} N/m^2 for HDPE at 165 °C. This value is close to the value (C = 1.23 X 10^{-9} N/m^2) obtained by Han and Drexler (Han & Drexler, 1973b) for HDPE.

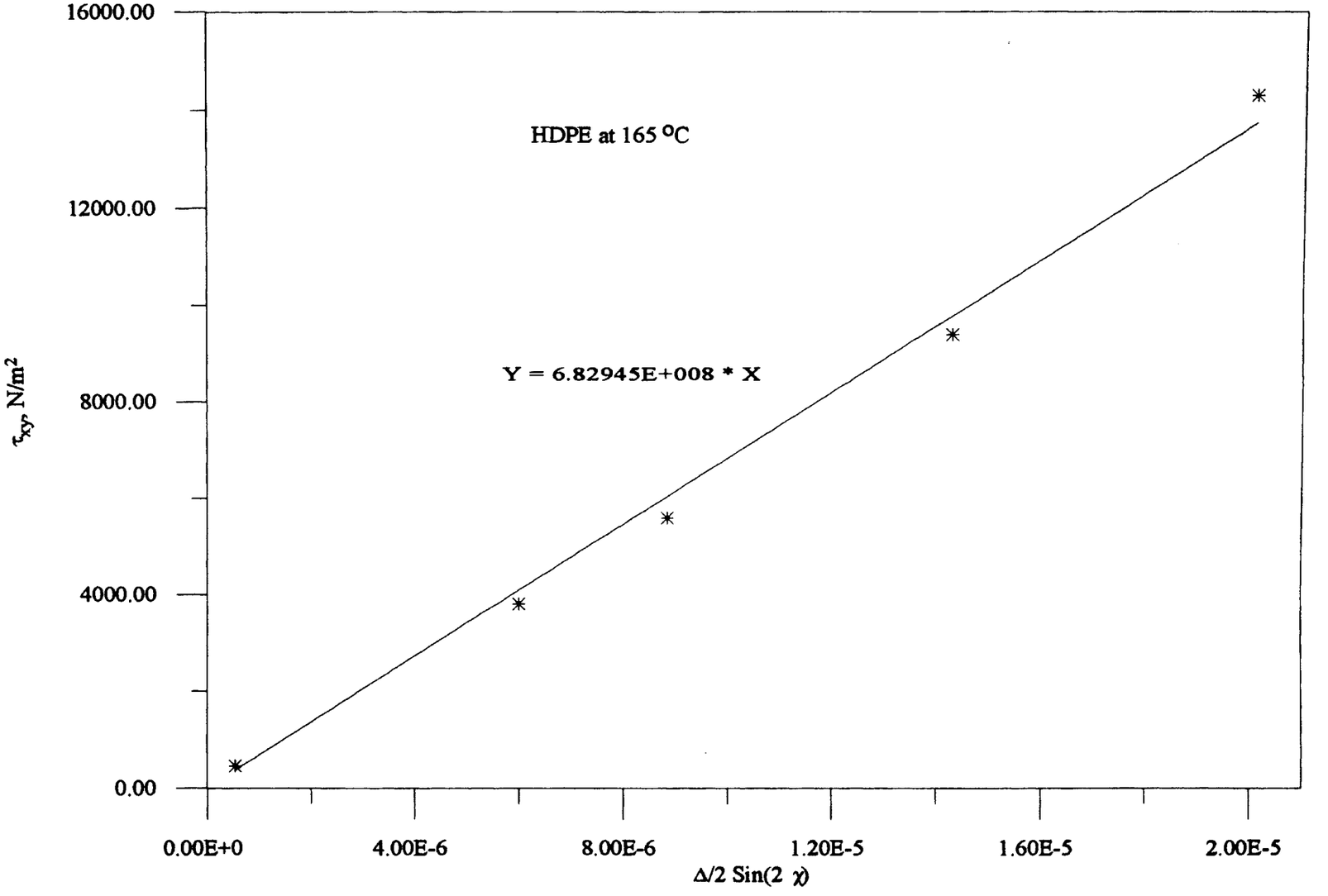

Fig 4.15: Calibration of C for HDPE at 165 °C

4.7 Stress Fields

From the isochromatic and isoclinic contours of Figures 4.13 and 4.14 contours of constant shear stress and first normal stress difference can be calculated using Eqs. 2.10 and 2.11. Results of the calculations for the shear stress and first normal stress difference are presented in Figures 4.16 and 4.17 for HDPE at 165 °C and 20 cc/min. The stress fields were presented only for the top half of the converging die since the die is symmetrical.

The shear stress contours in Figure 4.16 suggest that the shear stress is zero at the center line and reaches a maximum at the walls to the die and that the shear stress is inversely proportional to the distance from the slit flow entrance. These observations comply with the equation of continuity.

The first normal stress difference contours in Figure 4.17 suggest that the first normal stress difference is high near the walls of the channel and low near the center of the channel.

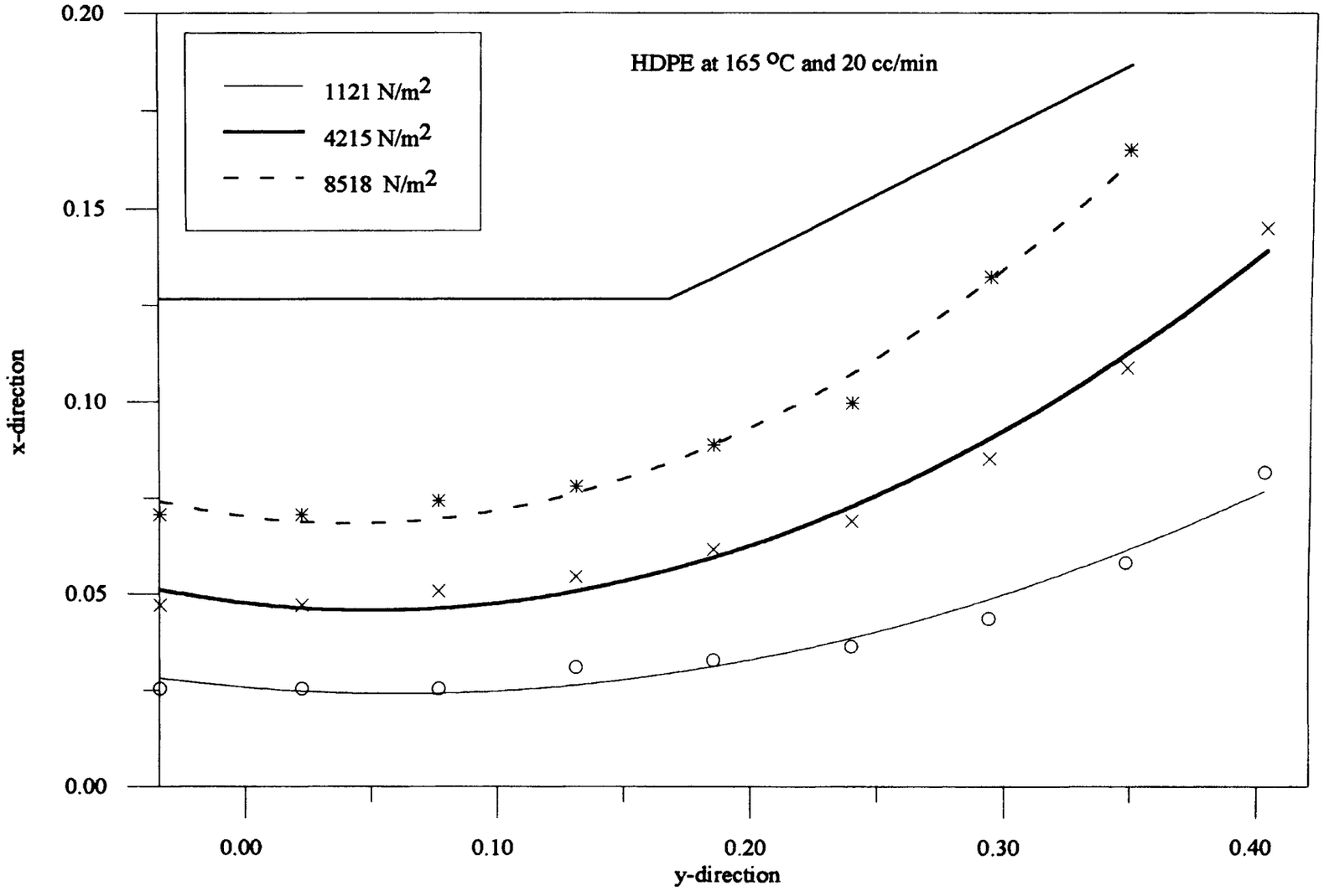

Fig 4.16: Shear Stress Contours in the Converging Channel

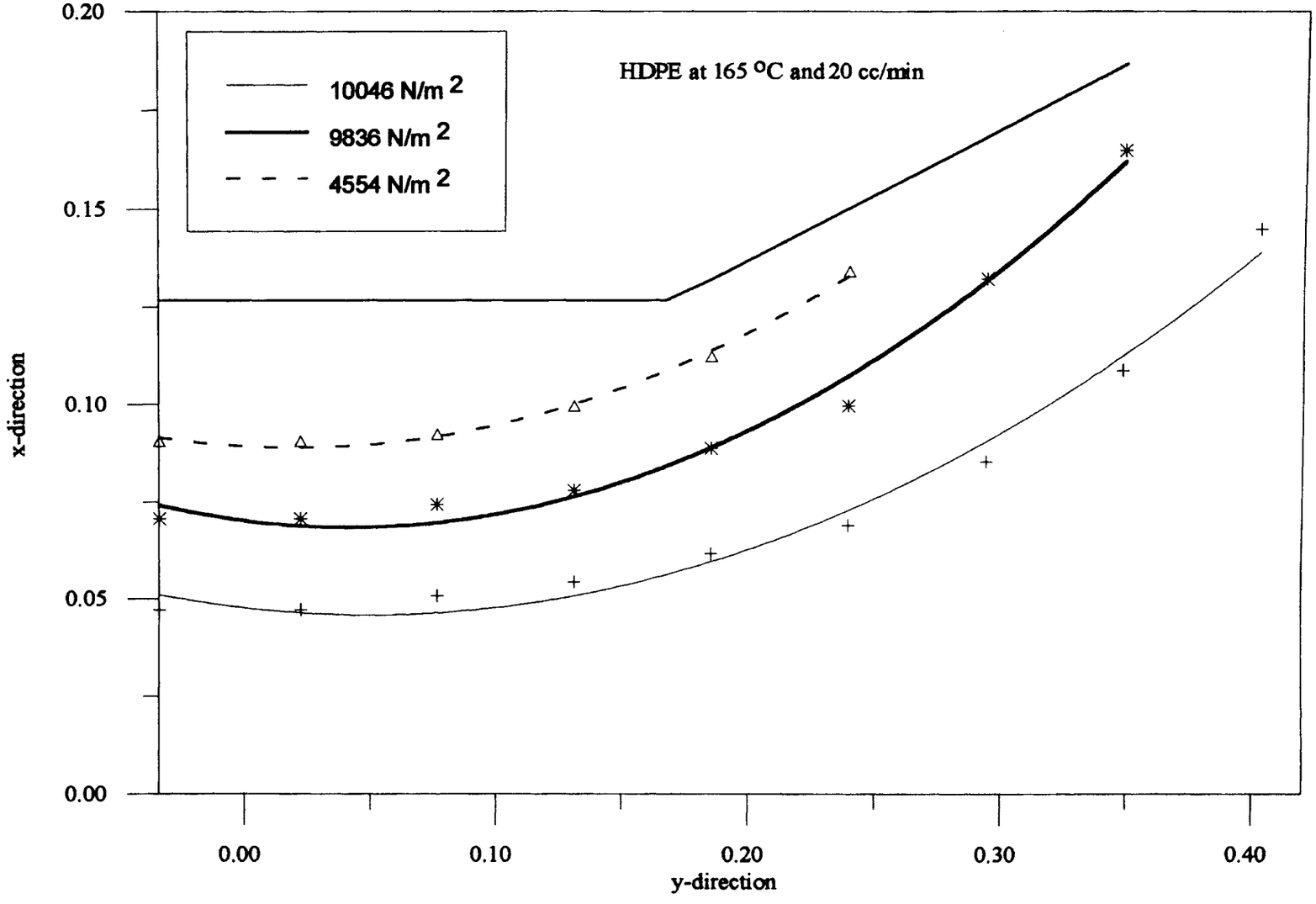

Fig 4.17: First Normal Stress Difference Contours in the Converging Channel

4.8 Flow Kinematics

The flow kinematics in the converging channel for HDPE at 165 °C and 20 cc/min were calculated using the functionality of stream function Ψ in the converging channel. The functionality of Ψ for HDPE at 165°C and 20 cc/min, in the converging channel is

$$\Psi = -2.63\eta^2+8.0\eta-5.82. \tag{4.32}$$

Eq. 4.32 was derived in Appendix F using the procedure given in Section 4.4. The different components of the rate of strain tensor are calculated from the Eqs. 4.24 and 4.25. Results of the calculations for shear strain rate and first normal strain rate difference are presented in Figure 4.18. From the figures it can be seen that the shear strain rate is minimum at the center of the channel and maximum at the walls. Also the shear strain rates increase immensely at mouth of the die. This behavior was expected as the velocity increases due to the decrease in flow area, and the velocity gradient at the mouth of the die is high. By looking at the shear stress contours it can be seen that both shear stresses and strain rates behave in the same way. From figure 4.18(b) it can be observed that the first normal strain rate difference is minimum at the wall and maximum at the center of the channel. One would expect a similar behavior for first normal stress difference. However from the first normal stress difference contours obtained from the birefringence data it can be seen that the first normal stress difference does not go through a zero in between the

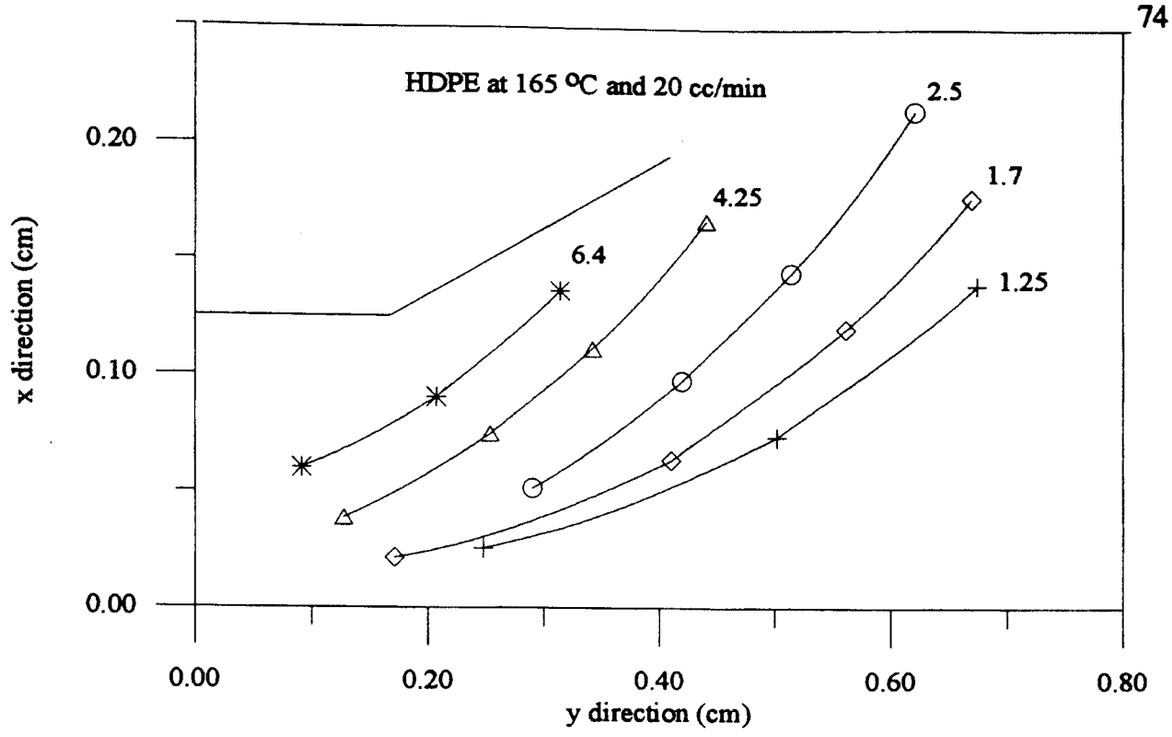

(a)

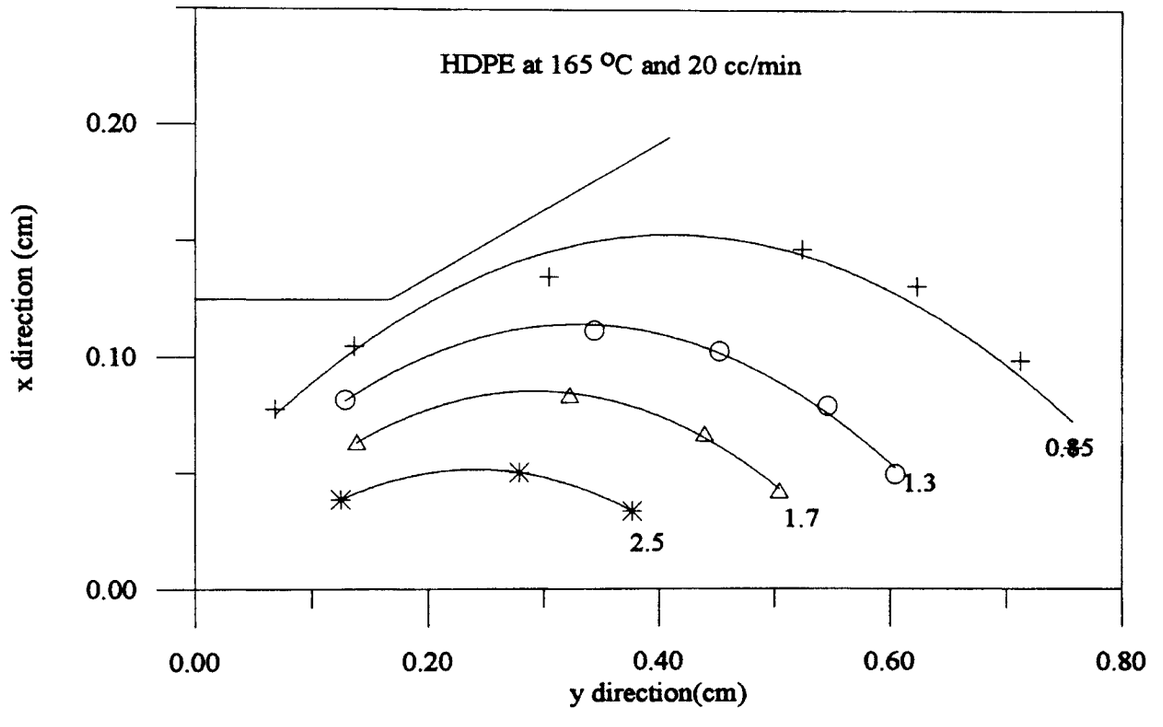

(b)

Fig. 4.18: Strain Rate Contours, a) Shear Strain Contours (sec^{-1})
b) First Normal Strain Difference Contours (sec^{-1})

wall and the center of the channel.

Based on the observations of the stress fields, a successful rheological equation of state must produce the following behavior for the kinematics presented in Figure 4.18:

(i) The center line of the die must be a zero shear stress contour;

(ii) The contour shapes of the shear stresses and first normal stress difference should match;

(iii) The shear stress should be maximum at the walls of the die;

4.9 Generalized Newtonian Fluids

In this section an attempt has been made to predict the stress fields from the kinematics using generalized Newtonian models. Figure 4.22 shows the predicted shear stress and first normal stress difference contours using a Newtonian constitutive equation and the flow kinematics from Section 4.8. The shear viscosity of HDPE was taken as 11800 N sec/m^2 as given by Han (Han & Drexler, 1973b). Figure 4.22 shows that the model predicts the shapes of the stress contours close to the experimental values but overestimates the values. This was expected as the model works only for Newtonian fluids. Figure 4.23 shows the prediction of stress fields by using a power law model and the flow kinematics. The power law indices for HDPE are taken as m= 11800 N sec^n/m^2 and n= 0.37 as given by Han and Drexler (Han & Drexler, 1973c). The predictions are better than a Newtonian fluid but the predicted values are still a magnitude more than the experimental values. Also the shape of the first normal stress difference contours could not be matched with the experimental results. So a higher order model would have to be used to be more accurate.

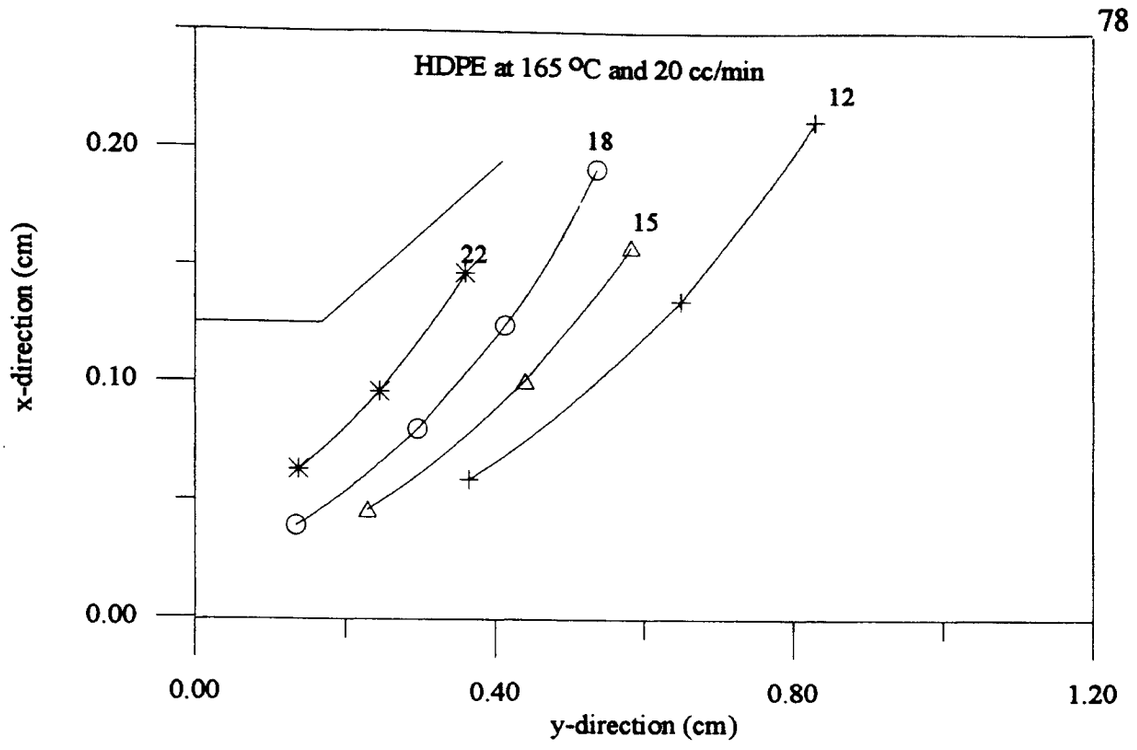

(a)

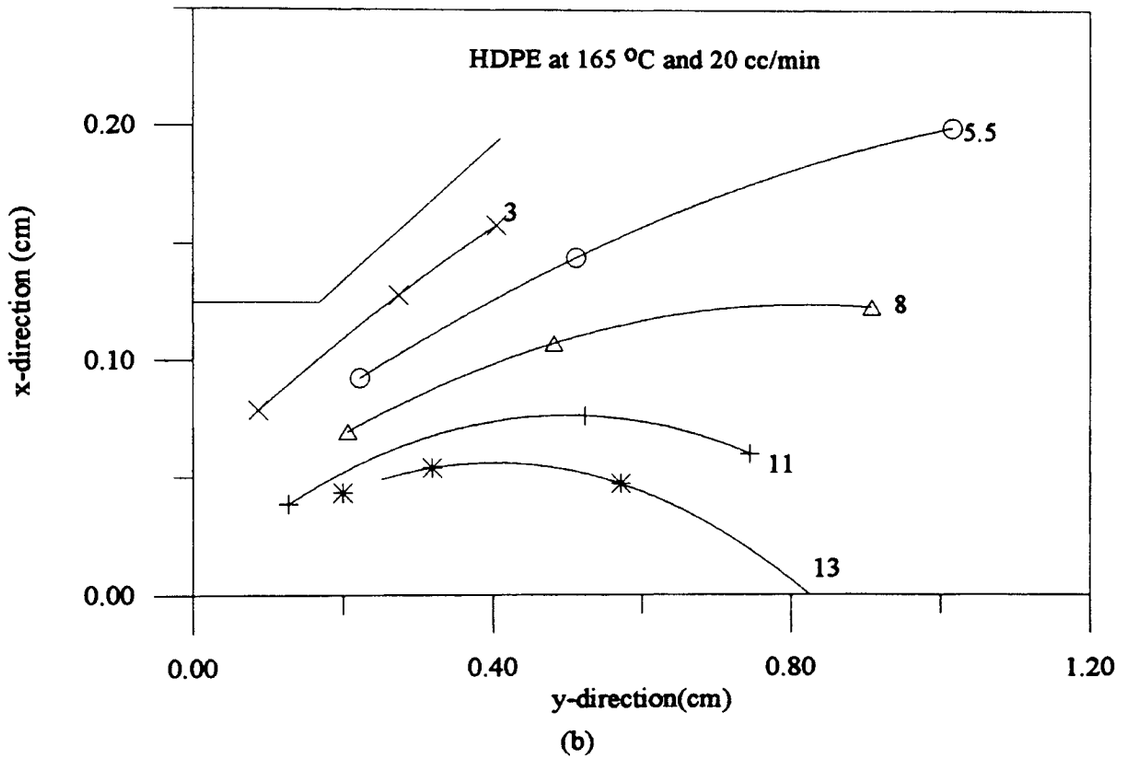

(b)

Fig. 4.20: Predictions Using the Power Law Model, a) Predicted Shear Stress Contours ($N/m^{2*}\ 10^3$) b) First Normal Stress Difference Contours ($N/m^{2*}\ 10^3$)

Chapter 5

SUMMARY, CONCLUSIONS AND RECOMMENDATIONS

5.1 Summary and Conclusions

The results of this thesis can be summarized as:

1. The ability of the elliptical cylindrical coordinate system to describe the stream lines in a converging channel has been demonstrated for one angle of convergence.
2. A theoretical consideration of the flow of polymer melts in converging channels using the elliptical cylindrical coordinate system was addressed.
3. The equation of motion, continuity equation and the spatial derivatives of unit vectors for the elliptical cylindrical coordinate system were derived.
4. The ability to calculate the flow kinematics using elliptical cylindrical coordinates was demonstrated and the functionality of the stream function was established.
5. The method of isoclinics was successfully used to calculate the stress optic coefficient of HDPE at 165 °C.
6. An extensive study on the abnormal behavior of the birefringence patterns, observed in the converging channel, was conducted.

7. A procedure to calculate the stress fields from these birefringence patterns was suggested.

8. The stress fields and strain rates were calculated independently in the converging channel for HDPE at 165 °C and flowing at a rate of 20 cc/min

The final aim of this project is to develop a rheological equation of state for mixed heterogenous polymer flow. This thesis made significant progress toward the study by accomplishing the following:

(i) Used a better coordinate system to calculate the flow kinematics more accurately

(ii) Derived all the equations necessary to work in that coordinate system

(iii) Demonstrated the ability to calculate independently the stress fields and flow kinematics

(iv) Formulated a method to calculate the flow kinematics more easily from volumetric flow rate and converging angle rather than using strenuous experimental procedures like tracer particle data or streak photography.

5.2 Recommendations

The following recommendations are made for the study of mixed heterogenous flow of polymer melts in a converging channel:

(i) Further study has to be carried out on flow birefringence behavior observed in this study to determine the position of the zero order isochromatic band more accurately. It is recommended that the field of vision of the camera is to be increased to have a

better view of the birefringence patterns.

(ii) The converging channel can be further studied by changing the converging angle channel to check if the elliptical cylindrical coordinates are convenient at different converging angles.

(iii) Correlate the kinematics from the tracer particle data and the stress data from birefringence to arrive at an rheological equation of state for mixed heterogenous flow.

(iv) Write a computer program to numerically solve Eq. 4.19 so that the flow kinematics can be determined easily. Also a better rheological model should be used for the analysis in Section 4.3.

(v) Further study should be carried on the significance of the c in Eq. 2.14 since the width of the converging channel at the mouth and value of c, seem to be connected.

BIBLIOGRAPHY

Ajai, S. S. (1992) Study of Mixed Heterogenous Flow Kinematics of Polymer Melts in Converging Channels. Masters, Oklahoma State University.

Bird, R.B., Armstrong, R.C., & Hassager, O. (1987). Dynamics of Polymeric Liquids, Vol 1, Fluid Mechanics. John Wiley & Sons.

Burghardt, W. G., & Fuller, G. G. (1989). End Effects of Flow Birefringence Measurements. Journal Of Rheology, 33(5), 771,779.

Cogswell, F. N. (1972). Converging Flow of Polymer Melts in Extrusion Dies. Polymer Engineering Science, 12(1), 64.

Froelich, D., Muller, R., & Zang, Y. H. (1986). New Extensional Rheometer for Elongational Viscosity and Birefringence Measurements: Experimental Results and Interpretation. Rubber Chemistry and Technology, 59(4), 564-573.

Galante, S. R., & Frattini, P. L. (1991). The Influence of End Effects on Birefringence Measurements in Nominally Two-Dimensional Channel Flows. Journal of Rheology, 35(8), 1551,1581.

Gortemaker, F. G., Cindio, B. D., & Janeschitz-Kriegl, H. (1976). Flow Birefringence of Polymer Melts:Calculation of Velocity and Temperature Profiles in cone and plate Apparatus. Reologica Acta, 15, 479,486.

Greener, J., & Machell, J. S. (1990). Rheo-Optical Properties of Polymer Blends. Polystyrene and poly(2,6-dimethyl- 1,4-phenylene oxide). Journal of Applied Polymer Science, 40, 1-2.

Guy, R. K. (1992) A Study Of Flow-Induced Crystallization In Two-Phase Polymer Melts. Doctoral, University of Illinois at Urbana-Champaign.

Han, C. D., & Drexler, L. H. (1973a). Studies of Converging Flows of Viscoelastic Polymeric Melts. I. Stress-Birefringent Measurements in the Entrance Region of a Sharp-Edged Slit Die. Journal of Applied Polymer Science, 17, 2329-2354.

Han, C. D., & Drexler, L. H. (1973b). Studies of Converging Flows of Viscoelastic Polymeric Melts. II. Velocity Measurements in the Entrance Region of a Sharp-Edged Slit Die. Journal of Applied Polymer Science, 17, 2355-2368.

Han, C. D., & Drexler, L. H. (1973c). Studies of Converging Flows of Viscoelastic Polymeric Melts. III. Stress and Velocity Distributions in the Entrance Region of a Tapered Slit Die. Journal of Applied Polymer Science, 17, 2369-2393.

Hsiao, B. S., Stein, R. S., Deutscher, K., & Winter, H. H. (1990). Optical Anisotropy of a Thermotropic Liquid Crystalline Polymer in Transient Shear. Journal of Polymer Science, Part B: Polymer Physics, 28(9), 1571-1588.

Hsiao, B. S., Winter, H. H., & Stein, R. S. (1989). Rheo-Optical Studies of a Thermotropic Liquid Crystalline Polyester. Polymer Reprints, Division of Polymer Chemistry, American Chemical Society, 30(2), 526-527.

Janeschitz-Kriegl, H. (1983). Polymer Melt Rheology and Flow Birefringence. Newyork: Springer-Verlag.

Kishbaugh, A. J. (1992) The Rheo-Optics Of Shear-Thickening and Structure Formation In Polymer Solutions. Doctoral, University of Illinois at Urbana-Champaign.

Kuhn, W., & Grun, F. (1942). Beziehungen Zwischen Elastischen Kostanten und Dehnungsdoppelbrechung Hochelasticher Stoffe. Kolloid Z., 101, 248.

Larson, R. G., Khan, S. A., & Raju, V. R. (1988). Relaxation of Stress and Birefringence in Polymers of High Molecular Weight. Journal of Rheology, 32(2), 145-161.

McHugh, A. J., Mackay, M. E., & Khomami, B. (1987). Measurement of Birefringence by the Method of Isoclinics. Journal of Rheology, 31(7), 619,634.

Park, H. J., Kiriakidis, D. G., & Mitsoulis, E. (1992). Birefringence Studies in Die Flows of an HDPE Melt. Journal of Rheology, 36(8), 1563-1583.

Picot, J. J. C., Santerre, J. P., & Wilson, D. R. (1989). Effect of Extensional and Shearing Strains on Molecular Orientation of a Polymer Melt. Polymer Engineering and Science, 29, 984-7.

Rajagopalan, D., Byars, J. A., Armstrong, R. C., & Brown, R. A. (1992). Comparison of Numerical Simulations and Birefringence Measurements in Viscoelastic Flow Between Eccentric Rotating Cylinders. Journal of Rheology, 36(7), 1349-1375.

Schunk, P. R., & Scriven, L. E. (1990). Constitutive Equation for Modeling Mixed Extension and Shear in Polymer Solution Processing. Journal of Rheology, 34(7), 1085,1119.

Subramanian, R., Wilson, D. R., & Picot, J. J. C. (1986). Flow Birefringence in Polymer Rheology.

Tree, D. A. (1990) Crystallization Kinetics of Polymer Melts in Extensional Flow. Doctoral, University of Illinois at Urbana-Champaign.

Treloar, L. R. G. (1975). The Physics of Rubber Elasticity (3 ed.). Oxford: Clarendon Press.

van Gurp, M., Breukink, C. J., Sniekers, R. J. W. M., & Tas, P. P. (1993). Rheological Characterization of Low Density Polyethylene in Planar Extension using Rheo-optics. Proceedings of Spie: The International Society for Optical Engineering, 2052, 297-304.

Wei, K. H., Nordberg, M. E., III, & Winter, H. H. (1987). Simulation of Planar Welding Flows: part 2. Strain History, Stress Calculation, and Experimental Comparison. Polymer Engineering and Science, 27(18), 1390-1398.

Yoo, H. J., & Han, C. D. (1981). Stress Distribution of Polymers in Extrusion Through a Converging Die. Journal of Rheology, 25(1), 115-137.

APPENDIX A

NOMENCLATURE

b	Channel half height
C	Stress Optic Coefficient
c	Constant associated Elliptical cylindrical coordinates
Ψ	Stream Function
Ψ_η	The partial derivative of Stream Function with respect to η
η	Constant Coordinate value in Elliptical Cylindrical System
ψ	Constant Coordinate value in Elliptical Cylindrical System
q_α	Curvilinear Coordinates
x_i	Cartesian Coordinates
h_α	Scale factor
δ	Unit vector
ρ	Density
v	Velocity
P	Pressure
g	Acceleration due to gravity
t	Present time

t'	Past time
N1	First normal stress difference
n_{p1}	First principle refractive index
n_{p2}	Second principle refractive index
α	Polarizer orientation angle
γ	The rate of strain tensor
τ	The stress tensor
τ_{11}	First normal shear stress
τ_{12}	Shear stress
τ_{22}	Second normal shear stress
χ	Isoclinic angle
χ_M	Orientation angle of the stress tensor
χ_0	Orientation angle of the refractive index tensor
λ	Wave length of light
T	Temperature
Tr	Transmittance
δ	Retardance

APPENDIX B

General Orthogonal Coordinates

The equations for general orthogonal coordinates presented here were taken from Bird, et al. (Bird, Armstrong, & Hassager, 1987).

Let the relation between cartesian coordinates x_i and the curvilinear coordinates q_α be given by

$$x_i = x_i(q_\alpha). \tag{B.1}$$

These can be solved for q_α to give the inverse relations.

The unit vectors in rectangular coordinates δ_i and the unit vectors in curvilinear coordinates δ_α are related as:

$$\delta_\alpha = \sum_i \frac{1}{h_\alpha}\left(\frac{\partial x_i}{\partial q_\alpha}\right)\delta_i, \tag{B.2}$$

$$\delta_i = \sum_\alpha \frac{1}{h_\alpha}\left(\frac{\partial x_i}{\partial q_\alpha}\right)\delta_\alpha, \tag{B.3}$$

where h_α the "scale factors" are given by

$$h_\alpha^2 = \sum_i \left(\frac{\partial x_i}{\partial q_\alpha} \right)^2 . \tag{B.4}$$

The spatial derivatives of the unit vectors δ_α are

$$\frac{\partial \delta_\alpha}{\partial q_\beta} = \frac{\delta_\beta}{h_\alpha} \frac{\partial h_\beta}{\partial q_\alpha} - \delta_{\alpha\beta} \sum_{\gamma=1}^{3} \frac{\delta_\gamma}{h_\gamma} \frac{\partial h_\alpha}{\partial q_\gamma} . \tag{B.5}$$

The ∇ operator is given by

$$\nabla = \sum_\alpha \frac{\delta_\alpha}{h_\alpha} \frac{\partial}{\partial q_\alpha} . \tag{B.6}$$

APPENDIX C

[∇v] in Elliptical Cylindrical Coordinates

The components of the tensor [∇v] in elliptical cylindrical Coordinates (ψ,η,z) were derived using the general equations in Appendix B and are given as:

$$\{\nabla v\}_{\psi\psi} = \frac{1}{h}\frac{\partial v_\psi}{\partial \psi} + \frac{v_\eta A}{h}, \tag{C.1}$$

$$\{\nabla v\}_{\psi\eta} = \frac{1}{h}\frac{\partial v_\eta}{\partial \psi} - \frac{v_\psi A}{h}, \tag{C.2}$$

$$\{\nabla v\}_{\psi z} = \frac{1}{h}\frac{\partial v_z}{\partial \psi}, \tag{C.3}$$

$$\{\nabla v\}_{\eta\psi} = \frac{1}{h}\frac{\partial v_\psi}{\partial \eta} - \frac{v_\eta B}{h}, \tag{C.4}$$

$$\{\nabla v\}_{\eta\eta} = \frac{1}{h}\frac{\partial v_\eta}{\partial \eta} + \frac{v_\psi B}{h}, \tag{C.5}$$

$$\{\nabla v\}_{\eta z} = \frac{1}{h}\frac{\partial v_z}{\partial \eta}, \tag{C.6}$$

$$\{\nabla v\}_{z\psi} = \frac{\partial v_\psi}{\partial z}, \tag{C.7}$$

$$\{\nabla v\}_{z\eta} = \frac{\partial v_\eta}{\partial z}, \tag{C.8}$$

$$\{\nabla v\}_{zz} = \frac{\partial v_z}{\partial z}. \tag{C.9}$$

APPENDIX D

Spatial Derivatives of the Unit Vectors in Elliptical Cylindrical Coordinates

The spatial derivatives of the unit vectors in Elliptical Cylindrical coordinate system were derived using the Eq. A.5 and are given as

$$\frac{\partial \delta_\psi}{\partial \psi} = -\frac{\delta_\eta}{2h^2} c \sin(2\eta), \tag{D.1}$$

$$\frac{\partial \delta_\eta}{\partial \psi} = \frac{\delta_\psi}{2h^2} c \sin(2\eta), \tag{D.2}$$

$$\frac{\partial \delta_\psi}{\partial \eta} = \frac{\delta_\eta}{2h^2} c \sinh(2\psi), \tag{D.3}$$

$$\frac{\partial \delta_\eta}{\partial \eta} = -\frac{\delta_\psi}{2h^2} c \sinh(2\psi), \tag{D.4}$$

$$\frac{\partial \delta_{\eta}}{\partial z} = \frac{\partial \delta_{\psi}}{\partial z} = 0, \tag{D.5}$$

$$\frac{\partial \delta_{z}}{\partial \psi} = \frac{\partial \delta_{z}}{\partial \eta} = \frac{\partial \delta_{z}}{\partial z} = 0. \tag{D.6}$$

APPENDIX E

Tracer Particle Data

This Appendix shows the tracer particle data which was fit to the following equation by the method of least squares

$$y^2 = x^2\tan^2\eta - C\sin^2\eta. \qquad \text{(E.1)}$$

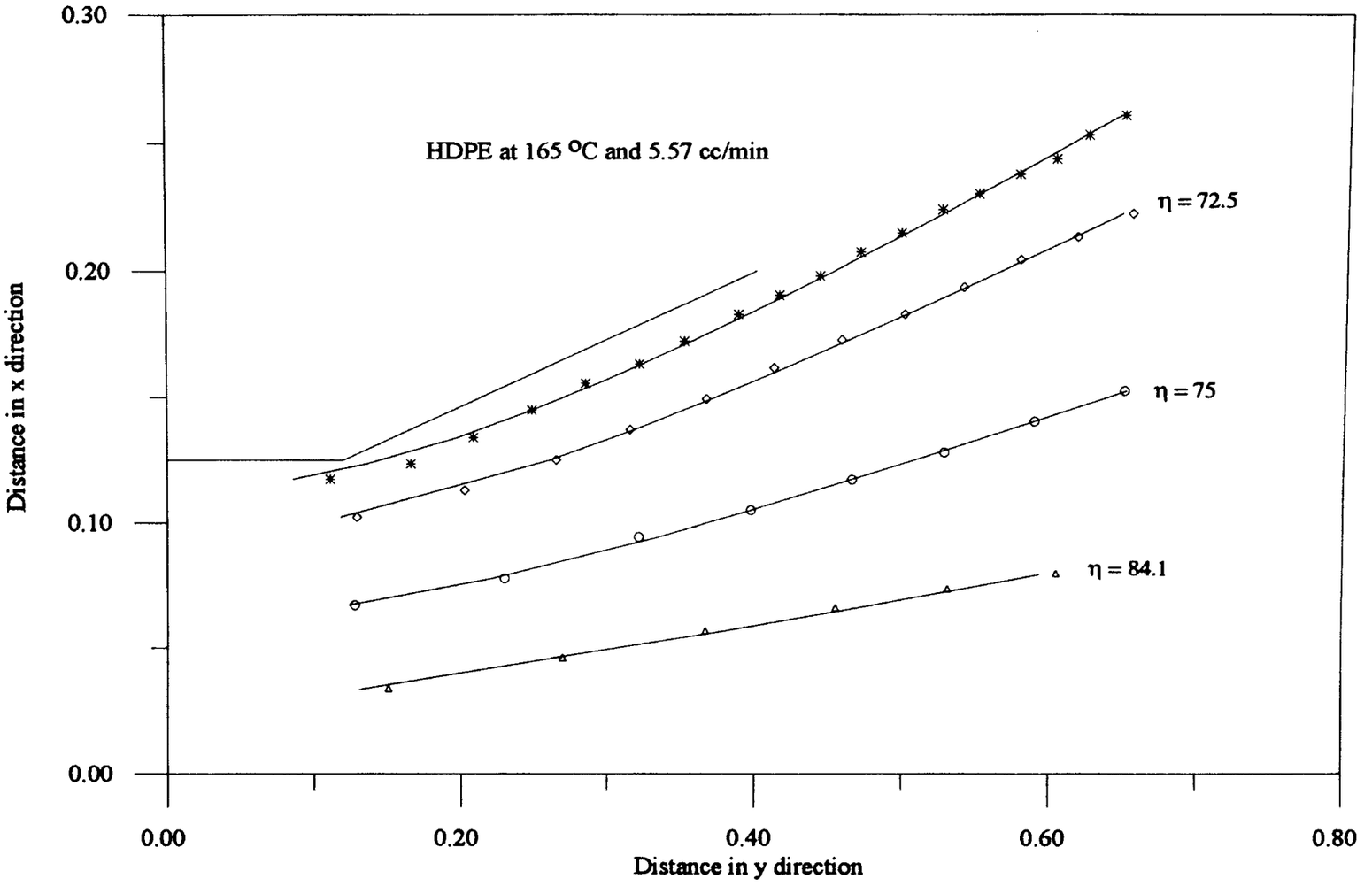

Fig E.1 : Streamlines Fit to Elliptic Cylindrical Coordinates

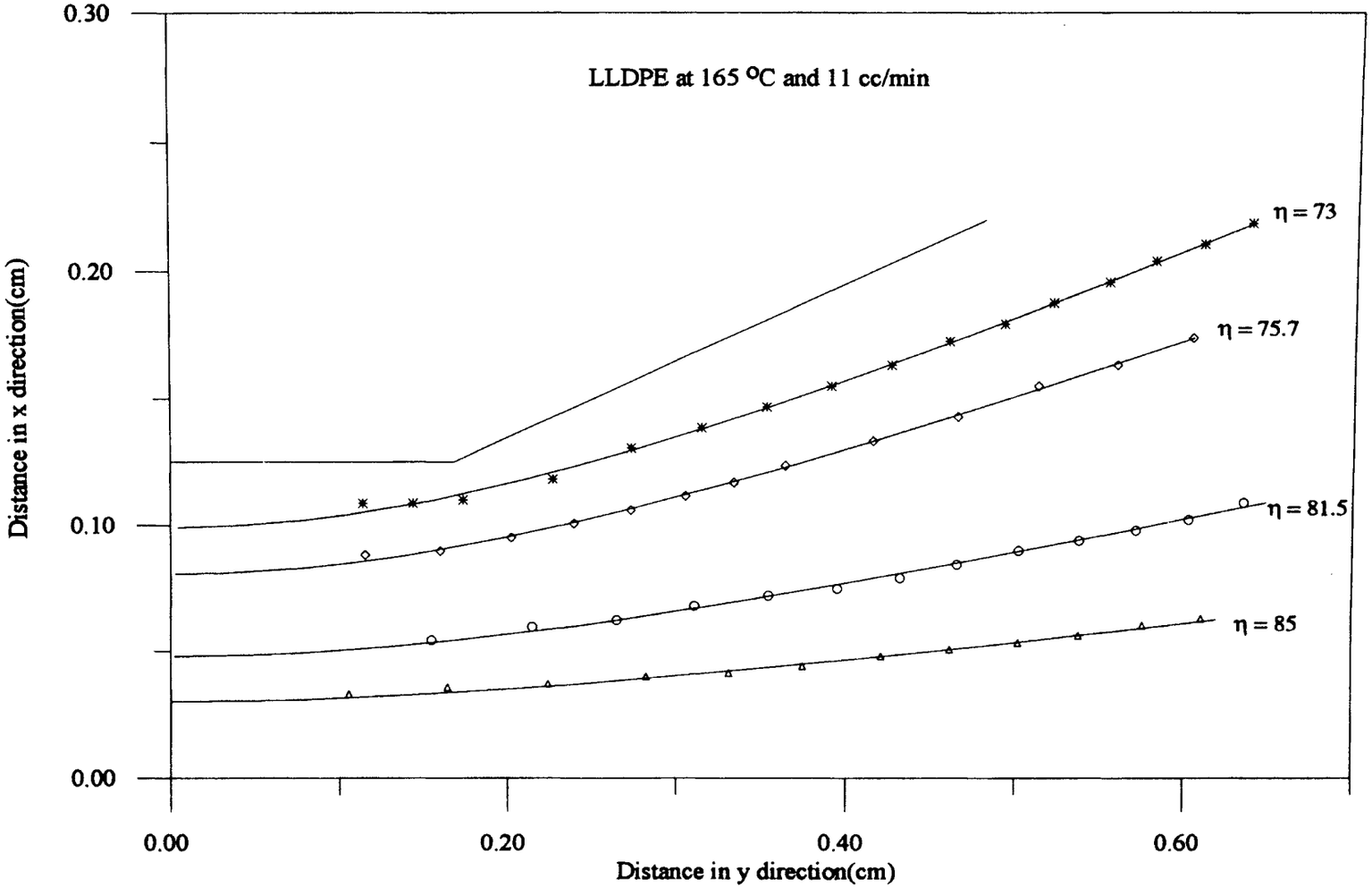

Fig E.2 : Streamlines Fit to Elliptic Cylindrical Coordinates

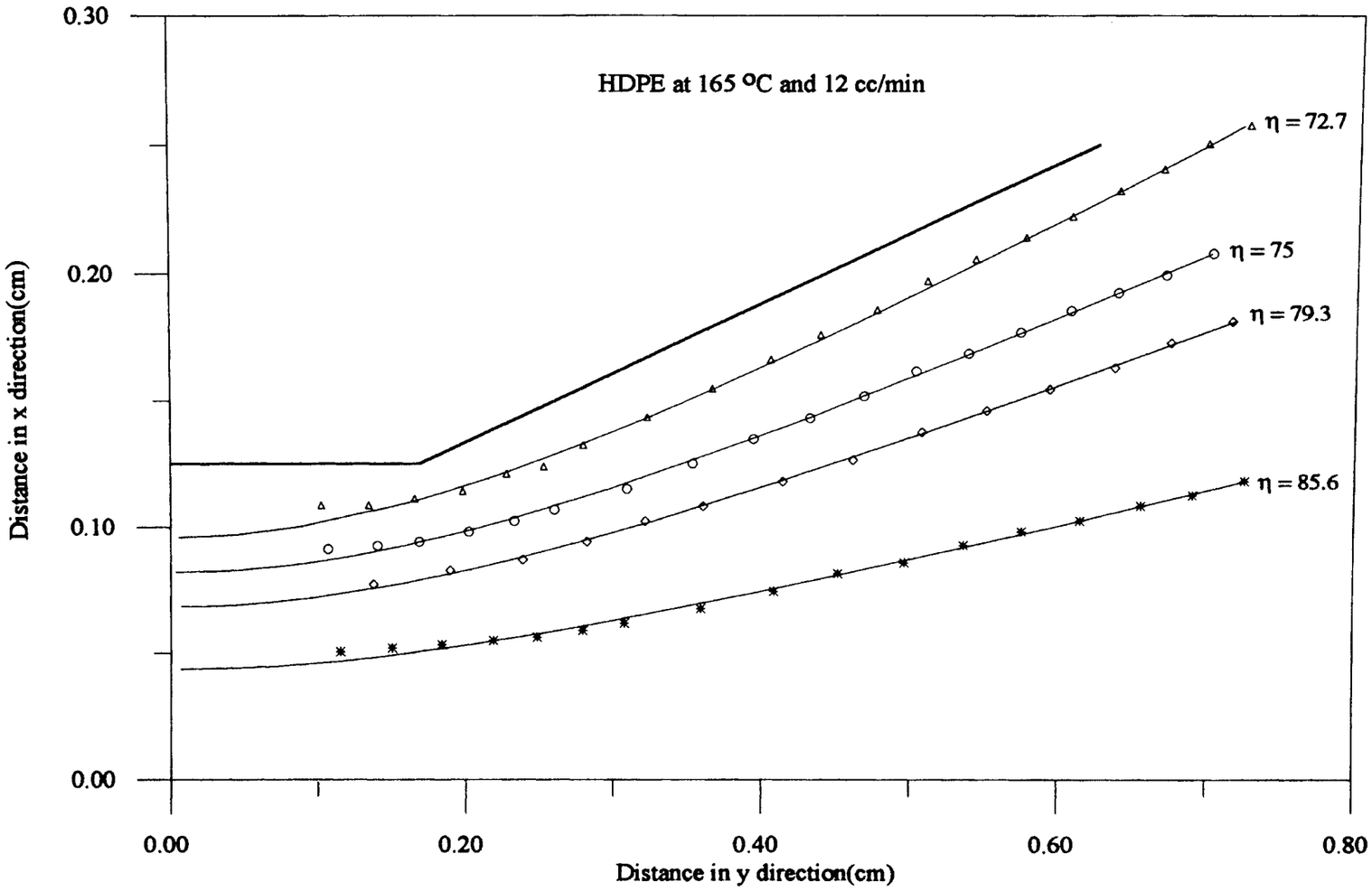

Fig E.3 :Streamlines Fit to Elliptic Cylindrical Coordinates

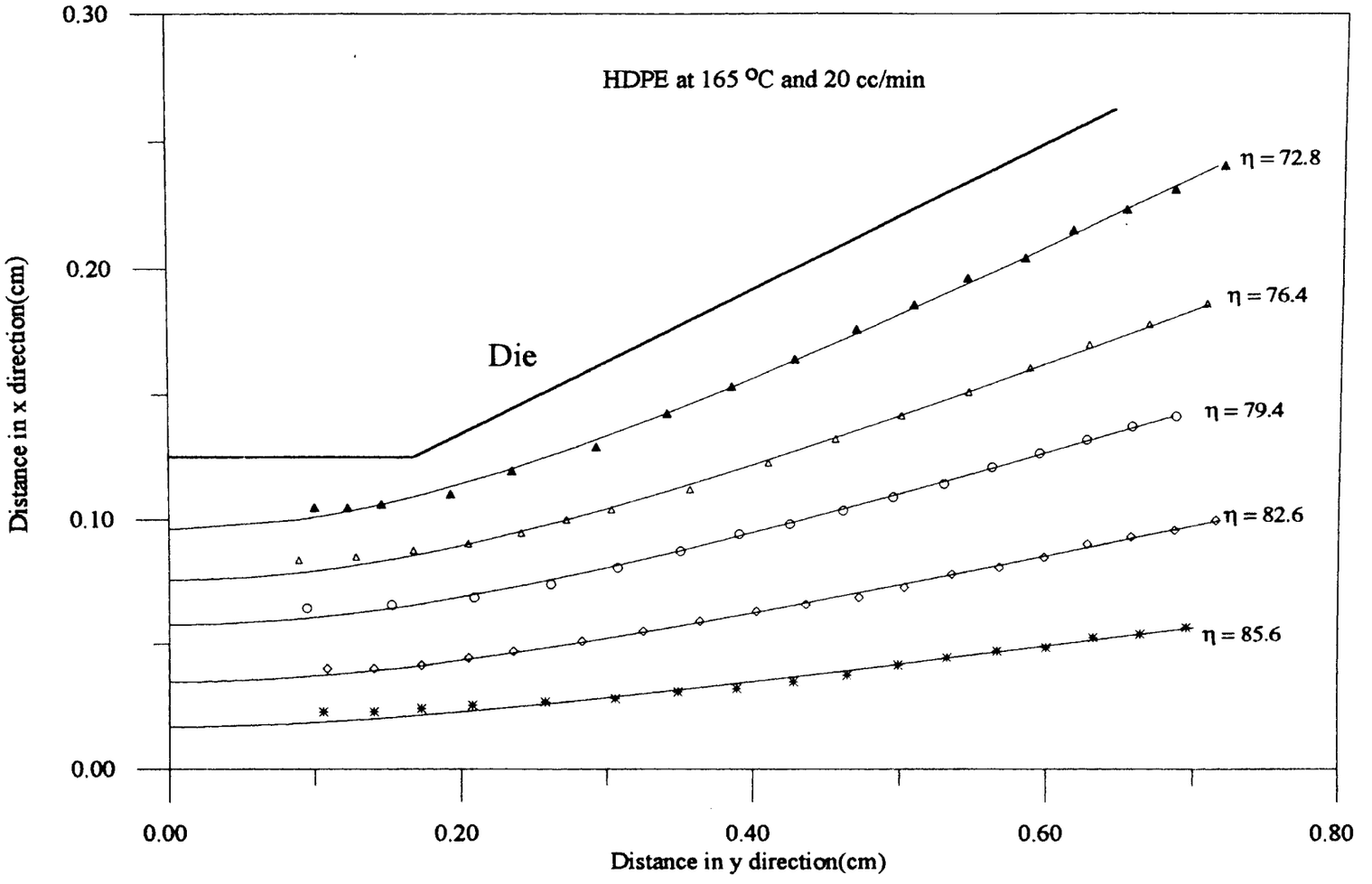

Fig E.4 : Stream lines fit to Elliptic Cylindrical Coordinates

APPENDIX F

Plots of Ψ vs η

This Appendix gives the tables of Ψ vs η, and the corresponding plots for HDPE at different temperatures and flow rates.

Converging Channel Kinematics

Ψ, cm^2/sec^{-1}	η, Rad
0.281	1.494
0.267	1.442
0.227	1.385
0.192	1.333
0.113	1.271

Table F.1 :Values of Ψ as a Function of η for HDPE at 165 °C and 20 cc/min

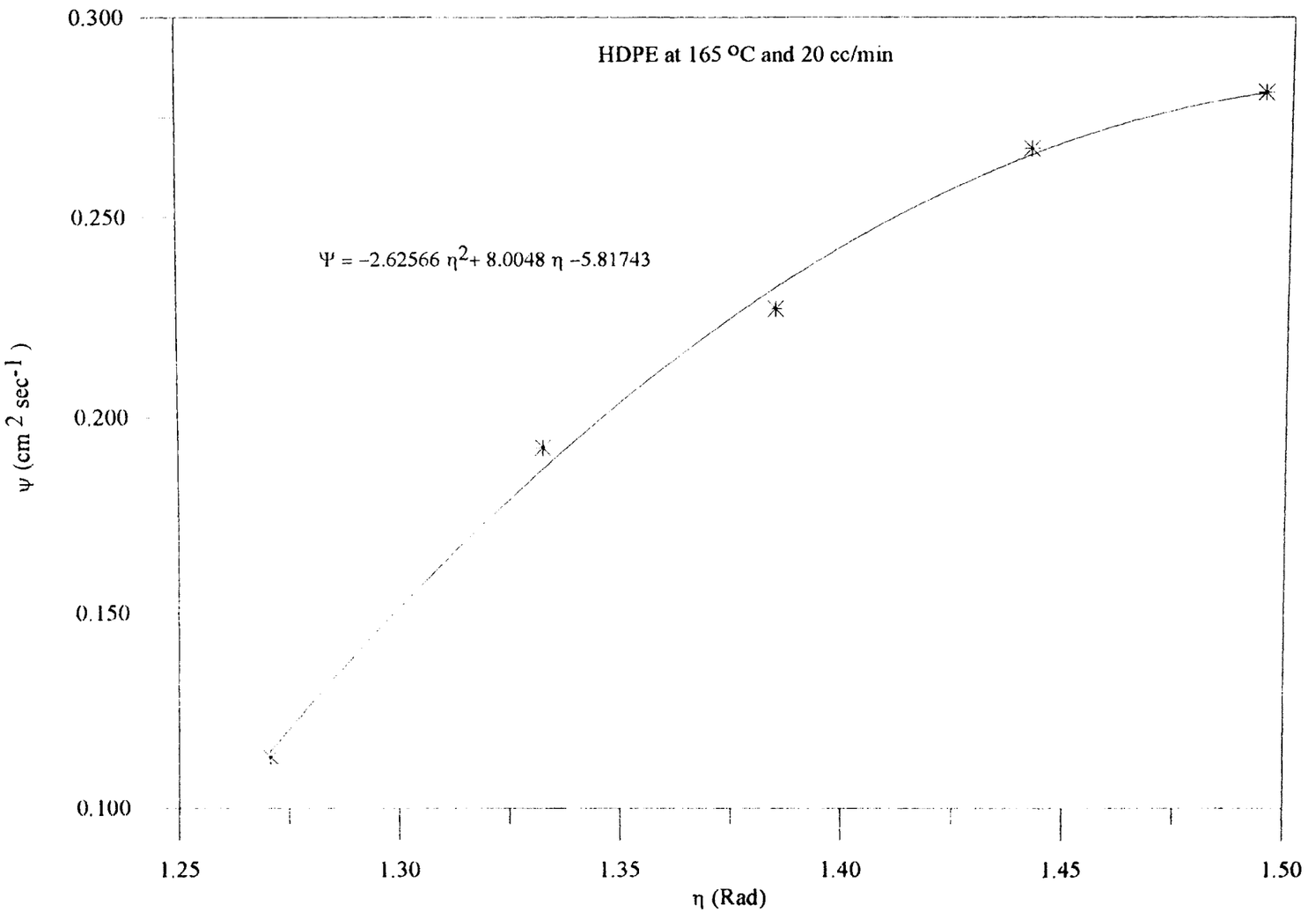

Fig F.1 : ψ as a Function of η for the Converging Channel

Converging Channel Kinematics

Ψ, cm^2/sec^{-1}	η, Rad
0.173	1.494
0.147	1.384
0.097	1.308
0.072	1.269

Table F.2 :Values of Ψ as a Function of η for HDPE at 165 °C and 12 cc/min

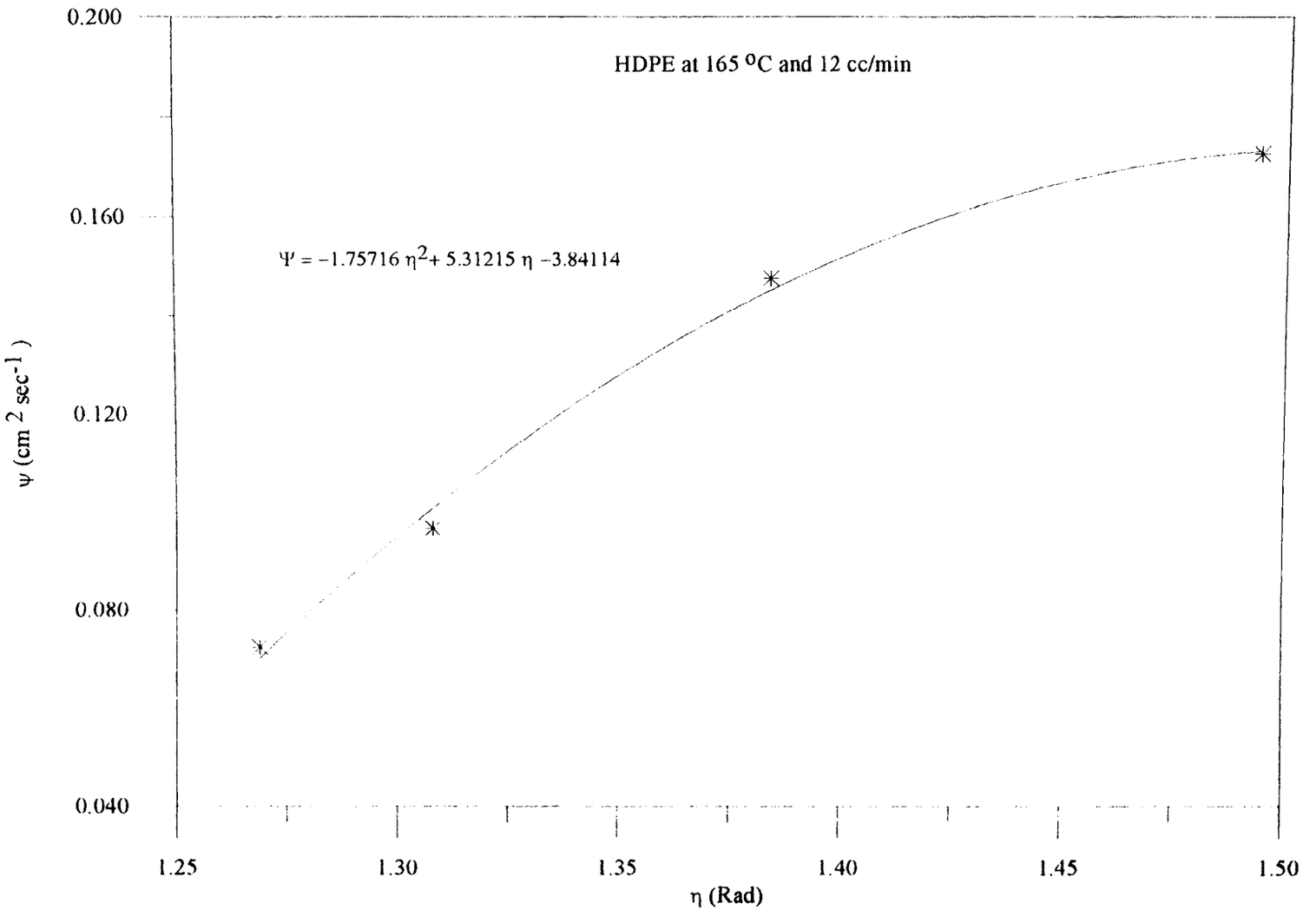

Fig F.2 : ψ as a Function of η for the Converging Channel

Converging Channel Kinematics

Ψ, cm^2/sec^{-1}	η, Rad
0.101	1.500
0.098	1.453
0.077	1.378
0.064	1.321
0.048	1.292
0.026	1.252

Table F.3 :Values of Ψ as a Function of η for HDPE at 165 °C and 6 cc/min

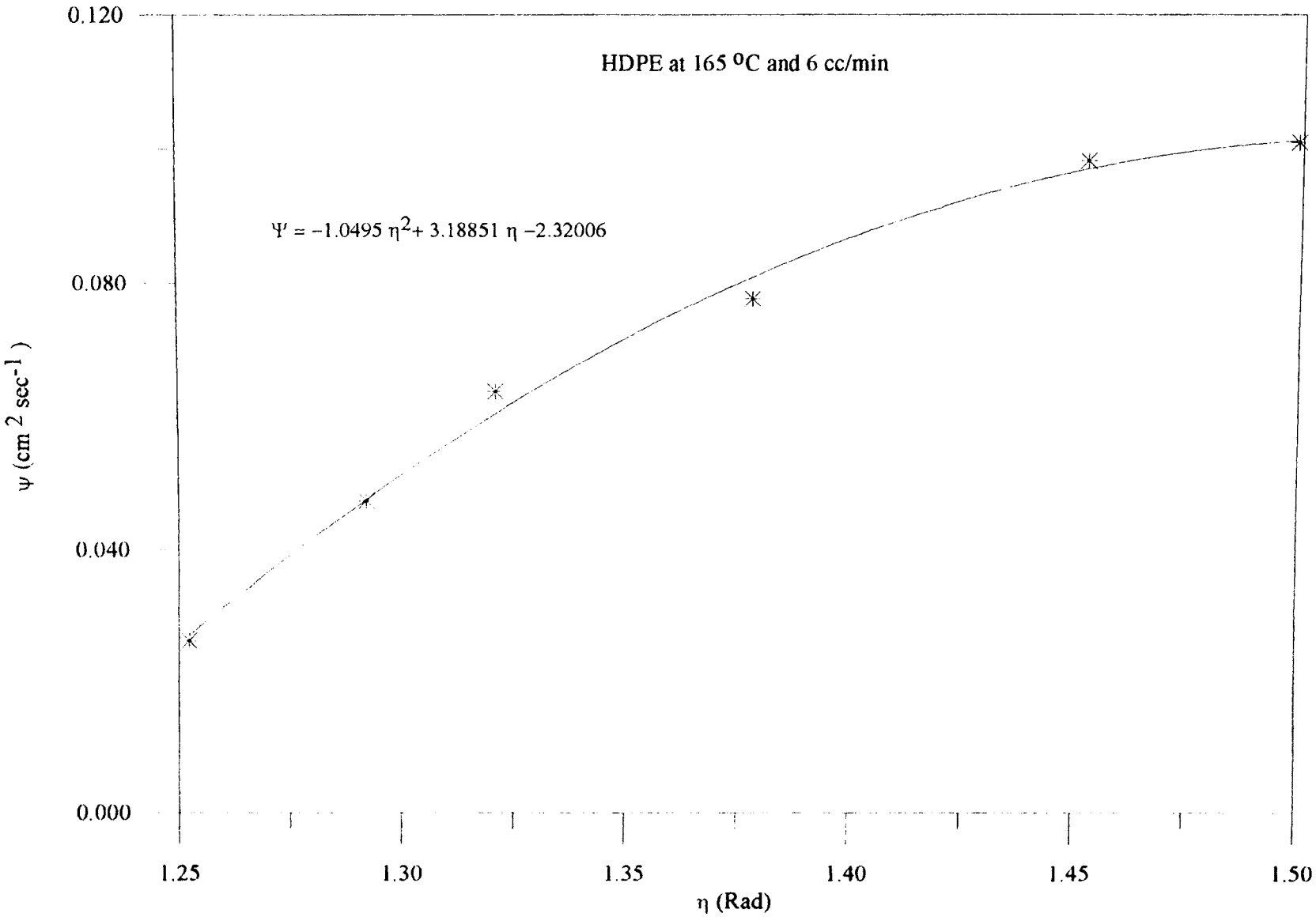

Fig F.3 : ψ as a Function of η for the Converging Channel

APPENDIX G

Light Transmission Equations

The equations that relate the intensity of light to the orientation, retardation, and dichroism needed in this study are presented in this chapter are taken directly from the work done by Tree and Guy (Tree, 1990; Guy, 1992). The state of light beam can be described completely, as it passes through each element of an optical train, by the stokes vector $\underline{B}$. This simplifies the determination of light transmission equation for these systems. This technique, called optical cascading, is performed in the following manner for an optical train with N elements and the order of multiplication to determine the final state of light is:

$$\underline{B} = \underline{E}_N \cdot \underline{E}_{N-1} \cdot \cdots \cdot \underline{E}_2 \cdot \underline{E}_1 \cdot \underline{B}_0 \qquad \text{(G.1)}$$

where

$\underline{E}_i$ = matrix of the iath element

$\underline{B}_0$ = Initial state of the light striking the first element.

A list of common optical elements and their Mueller matrices are given in Table G.1, and taken from the work by Guy (Guy, 1992). Thus for the case of two plane polarizers perpendicular to each other and a birefringent and dichroic element, the Stokes vector for the exiting light will be

Optical Element	Matrix
P(α), Ideal linear polarizer	$\frac{1}{2}\begin{bmatrix} 1 & C_{2\alpha} & S_{2\alpha} & 0 \\ C_{2\alpha} & C_{2\alpha}^2 & C_{2\alpha} & 0 \\ S_{2\alpha} & C_{2\alpha}S_{2\alpha} & S_{2\alpha}^2 & 0 \\ 0 & 0 & 0 & 0 \end{bmatrix}$
R(δ,χ), Pure retarder element	$\begin{bmatrix} 1 & 0 & 0 & 0 \\ 0 & C_{2\chi}^2+C_\delta S_{2\chi}^2 & S_{2\chi}C_{2\chi}(1-C_\delta) & S_\delta S_{2\chi} \\ 0 & C_{2\chi}S_{2\chi}(1-C_\delta) & S_{2\chi}^2+C_\delta C_{2\chi}^2 & -S_\delta C_{2\chi} \\ 0 & -S_\delta S_{2\chi} & S_\delta C_{2\chi} & C_\delta \end{bmatrix}$
M(δ,χ,κ), Coaxial dichroic and birefringent element	$e^{-A_c}\begin{bmatrix} Ch_\kappa & -Sh_\kappa C_{2\chi} & -Sh_\kappa S_{2\chi} & 0 \\ -Sh_\kappa C_{2\chi} & Ch_\kappa C_{2\chi}^2+C_\delta S_{2\chi}^2 & S_{2\chi}C_{2\chi}(Ch_\kappa-C_\delta) & S_\delta S_{2\chi} \\ -Sh_\kappa S_{2\chi} & C_{2\chi}S_{2\chi}(Ch_\kappa-C_\delta) & Ch_\kappa S_{2\chi}^2+C_\delta C_{2\chi}^2 & -S_\delta C_{2\chi} \\ 0 & -S_\delta S_{2\chi} & S_\delta C_{2\chi} & C_\delta \end{bmatrix}$

where $C_\beta = \cos(\beta)$, $S_\beta = \mathrm{Sin}(\beta)$, $Ch_\beta = \cosh(\beta)$, $Sh_\beta = \mathrm{Sinh}(\beta)$.

Table G.1 Mueller Matrices for Common Optical Elements

$$\underline{B} = P(\alpha+90^0)\cdot M(\delta,\chi,\kappa)\cdot P(\alpha)\cdot \underline{B}_0. \qquad \text{(G.2)}$$

Stokes vector for in coherent (non polarized light) can be given as

$$\underline{B}_0 = \begin{bmatrix} I_0 \\ 0 \\ 0 \\ 0 \end{bmatrix} \qquad \text{(G.3)}$$

where I_0 is incident light intensity. So the stokes vector can be calculated from Eq. G.2. While all four of the stokes parameters can be calculated, intensity I is the only parameter of interest in this study.

APPENDIX H

Significance of the Terms c and η in Elliptical Cylindrical Coordinates

In this appendix a study on how the stream lines differ with change in η and c values in Eq. 2.14, is presented. The η values vary from 90^0 to 70^0 and the c values vary from .016 to 1. These particular values were used since the converging angle limits the η and the c values of the experimental data in Appendix E were in this range. Figure H.1 gives a family of stream lines for different η when the value of c is fixed. Figure H.2 shows how the stream lines vary as c is changed. Figure H.2 shows that the curvature of the stream lines increase as the c value is increased. Also the effect of c value is more prominent at lower η. When c is zero in Eq. 2.14 the equation becomes similar to equation for stream line in cylindrical coordinates. Therefore the term c gives the elliptical cylindrical coordinates the ability to describe the curvy nature of the stream lines at the slit flow entrance. Figure H.1 shows that by using a right value of c for set of stream lines, the stream lines can be well represented by using η alone. For example when c is 0.075 the stream lines shown resemble the experimental data. Further studies have to be carried on how to arrive at an optimum c value for a system and fit the tracer particle data with Eq. 2.14 using fixed c.

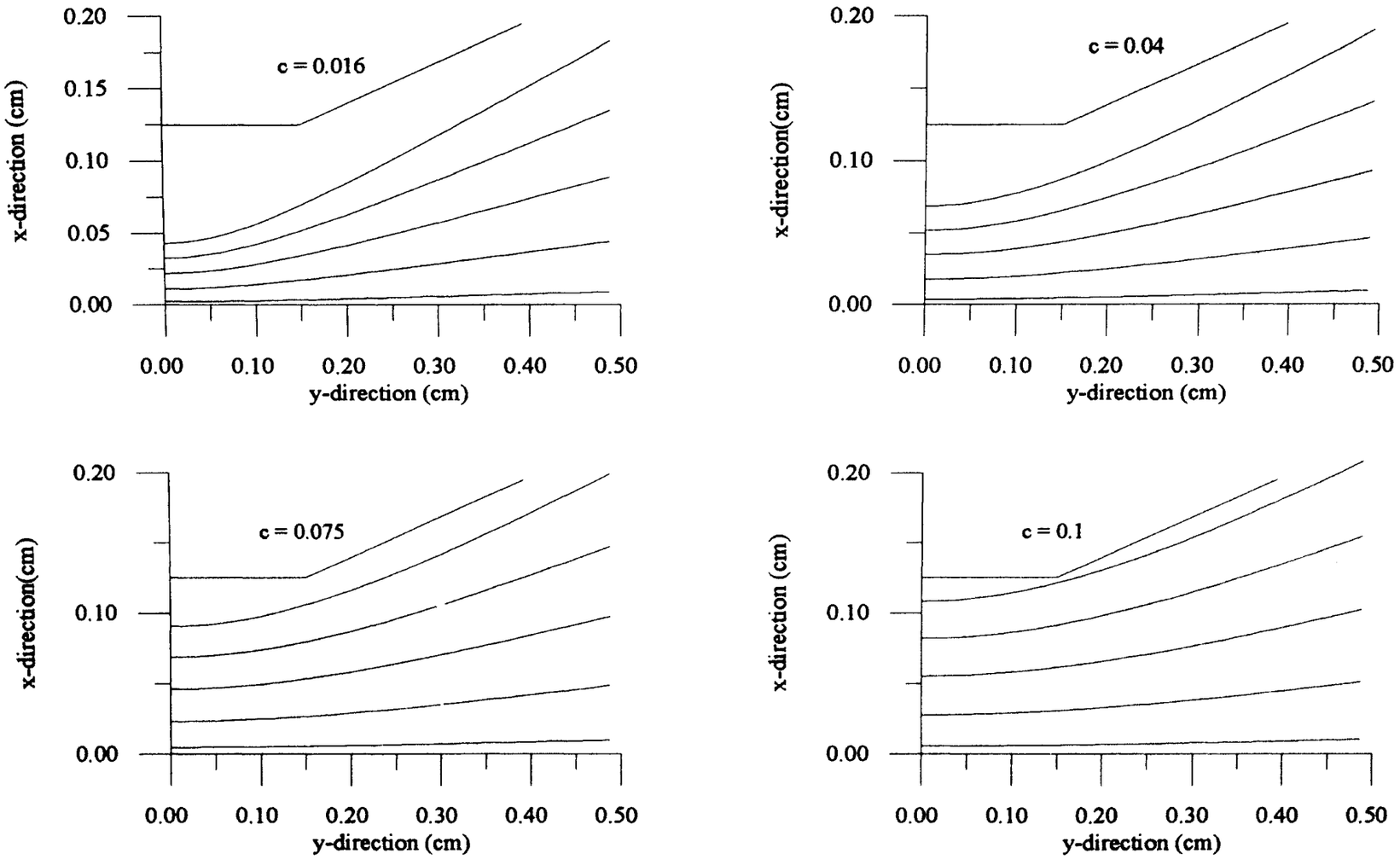

Fig H.1 : Streamlines with Change in c for Different η(89, 85, 80, 75, 70)

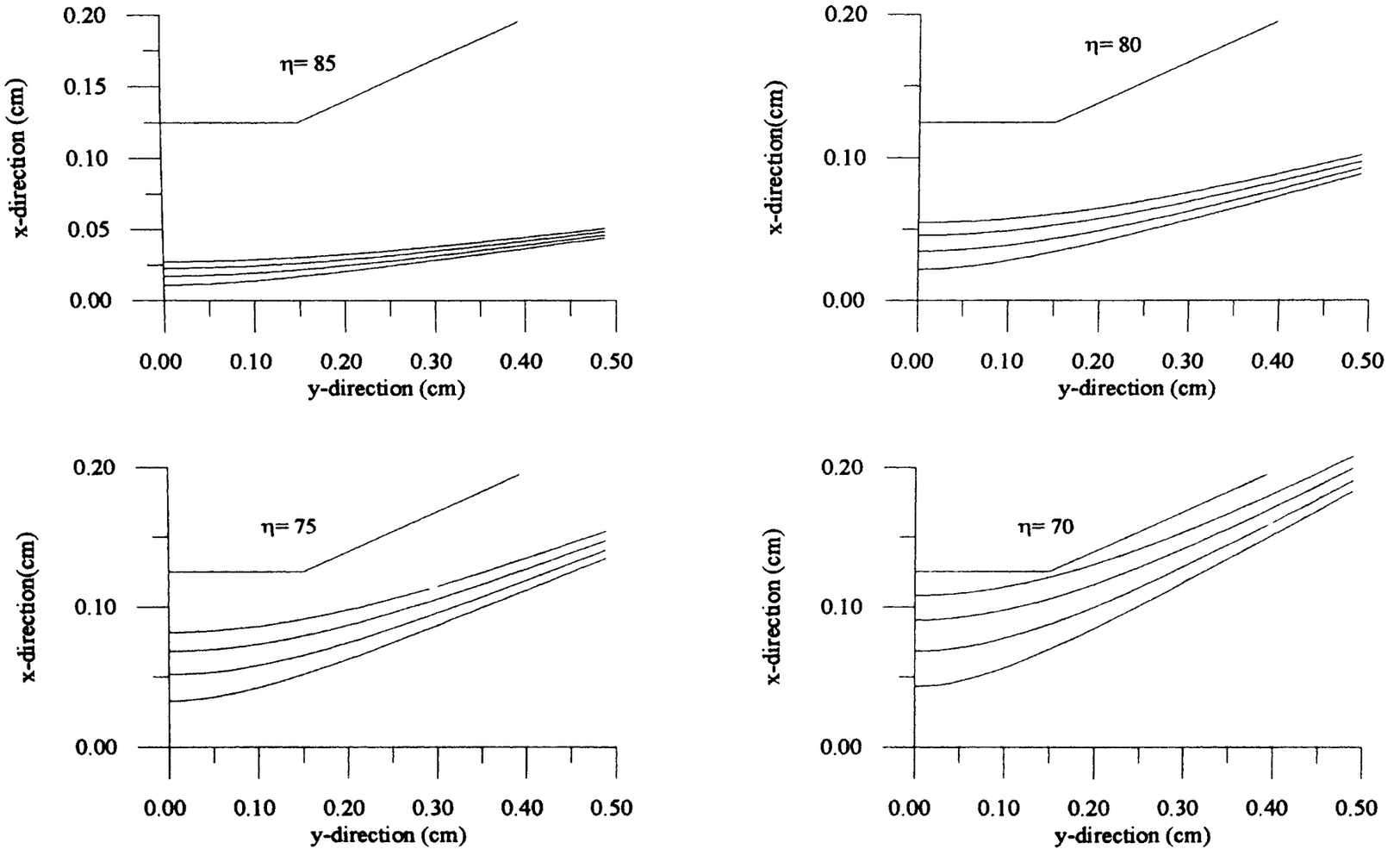

Fig H.2 : Streamlines with Change In ηfor Different C (0.016, 0.04, 0.07, 0.1)

VITA

Rajasekhar Mallipeddi

Candidate for the Degree of

Master of science

Thesis:STUDY OF MIXED, HETEROGENOUS FLOW OF POLYMER MELTS IN A CONVERGING CHANNEL DIE USING ELLIPTICAL CYLINDRICAL COORDINATES

Major Field: Chemical Engineering

Biographical:

Personal Data: Born in Tenali, Andhrapradesh, India, April 2, 1971, the son of Sivaprasada Rao Mallipeddi and Sujata Mallipeddi.

Education: Graduated from Sri Venkateswara Junior College, Tirupati, India, in May 1988; received Bachelor of Technology degree in Chemical Engineering from the Regional Engineering College, Tiruchirapalli, India in April, 1992; completed requirements for the Master of Science degree at the Oklahoma State University in December, 1994.

Professional Experience: Teaching Assistant, Department of Chemical Engineering, Oklahoma State University, August, 1992, to December, 1993; Tutor, Multicultural Development and Assessment center, Oklahoma State University, October, 1993, to May 1994.